

Supporting Information for  
**Efficient Copolymerization of Acrylate and Ethylene with Neutral  
P, O-Chelated Nickel Catalysts: Mechanistic Investigations of  
Monomer Insertion and Chelate Formation**

Shuoyan Xiong<sup>†1</sup>, Manar M. Shoshani<sup>†1</sup>, Xinglong Zhang<sup>†1</sup>, Heather A. Spinney<sup>2</sup>, Alex J. Nett<sup>2</sup>, and Briana S. Henderson<sup>2</sup>, Thomas F. Miller III<sup>\*1</sup>, and Theodor Agapie<sup>\*1</sup>

\*To whom correspondence should be addressed, E-mail: agapie@caltech.edu,  
tfm@caltech.edu

<sup>1</sup>*Division of Chemistry and Chemical Engineering, California Institute of Technology, Pasadena, California 91125, United States*

<sup>2</sup>*Chemical Science, Core R&D, Dow, Midland, Michigan 48667, United States*

***Experimental details for***

***Part A: Ligands and metal complexes***

1. Synthesis of ligands and metal complexes	S2
2. NMR characterization of ligands and metal complexes	S16
3. Solution-state NMR characterization and discussion of <b>5</b>	S26
4. Crystallographic information	S31

***Part B: Ethylene/tBA copolymerization***

5. Conditions and results.	S38
6. NMR Characterization of ethylene/tBA copolymers	S47
7. GPC curves of ethylene/tBA copolymers	S51

***Part C: Kinetic studies***

8. Kinetic measurements	S54
9. DFT calculations	S76
10. Computational investigation in isomerization	S112
11. Discussion of experimental and computational kinetic studies	S121

<i>References</i>	S129
-------------------	------

## 9. DFT calculation

### 9.0 Computational Methods

Geometry optimizations in the gas phase were initially carried out using the GFN1-xTB method<sup>8</sup> as implemented in Entos Qcore Version 0.7.<sup>9</sup> The resulting structures were further optimized using hybrid meta-generalized gradient-approximation (hybrid meta-GGA) M06 functional<sup>10</sup> with Karlsruhe-family basis set of double- $\zeta$  valence def2-SVP<sup>11,12</sup> for all atoms as implemented in *Gaussian 16* rev. A.03.<sup>13</sup> Where possible, available X-ray crystal structures were used as an initial guess. The M06 functional was chosen as it performs better than many other functionals (e.g.  $\omega$ B97X-D and TPSS) in predicting transition metal (TM) reaction barrier heights (TMBH21 dataset)<sup>14-16</sup> for reactions involving TMs.<sup>3,17</sup> M06 has also been employed to study similar TM-catalyzed systems with excellent agreement with experimental results.<sup>18,19</sup> Minima and transition structures on the potential energy surface (PES) were confirmed as such by harmonic frequency analysis, showing respectively zero and one imaginary frequency, at the same level of theory. Where appropriate, intrinsic reaction coordinate (IRC) analyses<sup>20,21</sup> were performed to confirm that the found TSs connect to the right reactants and products.

Single point (SP) corrections were performed using M06 functional and def2-TZVP<sup>11</sup> basis set for all atoms. The implicit SMD continuum solvation model<sup>22</sup> was used to account for the solvent effect of chlorobenzene on the Gibbs energy profile. Gibbs energies were evaluated at the reaction temperature of 323.15 K, using a quasi-RRHO treatment of vibrational entropies.<sup>23,24</sup> Vibrational entropies of frequencies below 100 cm<sup>-1</sup> were obtained according to a free rotor description, using a smooth damping function to interpolate between the two limiting descriptions. The free energies were further corrected using standard concentration of 1 mol/L, which was used in solvation calculations. SMD(chlorobenzene)-M06/def2-TZVP//M06/def2-SVP Gibbs energies are given and quoted in kcal mol<sup>-1</sup> throughout. *Unless otherwise stated, these solvent-corrected values are used for discussion throughout the main text and in this supporting information.*

Non-covalent interactions (NCIs) were analyzed using NCIPLOT<sup>25</sup> calculations. The *.wfn* files for NCIPLOT were generated at M06/DGDZVP<sup>26,27</sup> level of theory. NCI indices calculated with NCIPLOT were visualized at a gradient isosurface value of  $s = 0.5$  au. These are colored according to the sign of the second eigenvalue ( $\lambda_2$ ) of the Laplacian of the density ( $\nabla^2\rho$ ) over the range of -

0.1 (blue = attractive) to +0.1 (red = repulsive). Molecular orbitals are visualized using an isosurface value of 0.05 throughout. All molecular structures and molecular orbitals were visualized using *PyMOL* software.<sup>28</sup> Geometries of all optimized structures (in *.xyz* format with their associated energy in Hartrees) are included in a separate folder named *structures\_xyz* with an associated README file. All these data have been deposited with this Supporting Information. All Python scripts used for data analysis are taken from <https://github.com/bobbypaton>.

### 9.0.1 Conformational considerations

Where available, experimentally obtained X-ray crystal structures were used as initial guess for geometry optimization. Where different conformers exist in the X-ray structures, all available conformers were used for geometry optimization and the final optimized, lowest energy structure is used. The ligand backbone from the lowest energy conformer is then kept fixed for all subsequent reaction paths. For olefin insertions, all possible coordination modes/orientations were considered in the geometry optimization and the lowest energy conformers are used for discussion.

## 9.1 Reaction pathways leading from POP-Ni-py (1)

### 9.1.1 The starting structure of POP-Ni-py (1)

The starting structure for the optimization of **POP-Ni-py** complex was taken from the experimentally obtained X-ray crystal structure. The henceforth optimized structure **1-c2** is shown in Figure S9.1. We found another optimized structure (**1**) that is lower in energy than **1-c2** and we take this as the zero energy reference for this reaction (Figure S9.1). Note that these two structures are essentially conformers and they differ in the spatial orientation of the trialkylsilylated polymer chain.

<b>1</b>	<b>1-c2</b>
$\Delta G = 0.0$	$\Delta G = 9.8$

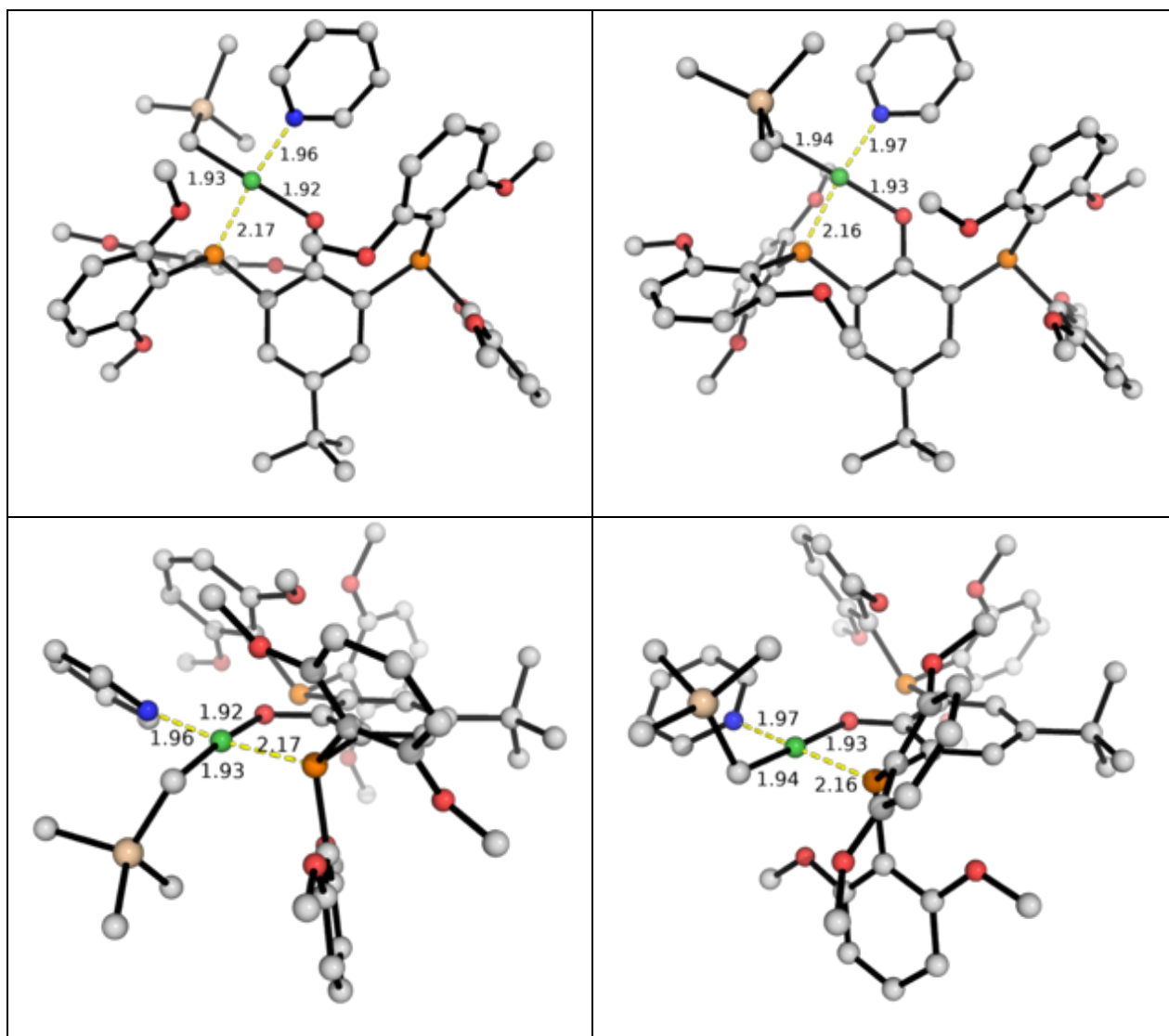


**Figure S9.1.** Optimized structures for the Ni(II) complex **POP-Ni-py**. The Gibbs energies are calculated at SMD (chlorobenzene)-M06/def2-TZVP//M06/def2-SVP level of theory and measured relative to the most stable species (**1**). Key bond distances are given in Å. Gibbs energy units are given in kcal mol<sup>-1</sup>.

### 9.1.2 Ethylene-bound Ni(II) complex – displacement of pyridine by ethylene in POP-Ni-py

<b>int1-et-c1</b>	<b>int1-et-c2</b>
$\Delta G = 8.9$	$\Delta G = 14.8$

**Figure S9.2.** Optimized structures for the Ni(II) complex **POP-Ni-et**. The Gibbs energies are calculated relative to **POP-Ni-py** (**1**). Key bond distances are given in Å. Gibbs energy units are given in kcal mol<sup>-1</sup>.

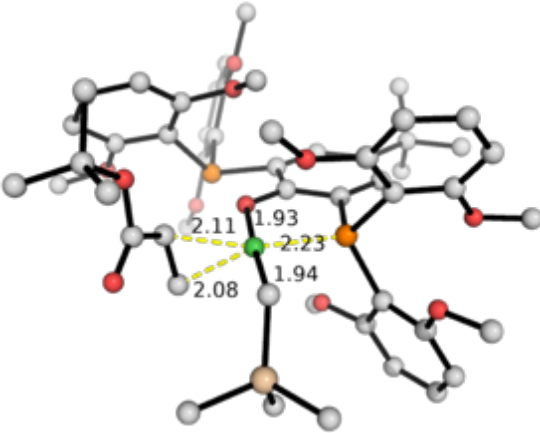
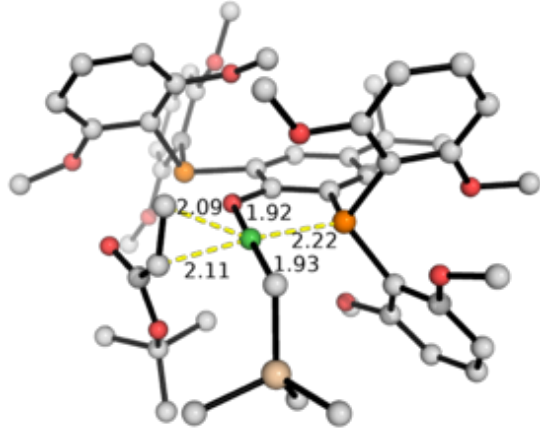
Herein we show the optimized structures of the Ni(II) complex where the pyridine ligand gets displaced by ethylene substrate. We denote these as **POP-Ni-et** complexes where the suffix “**et**” denotes ethylene. Two structures can be found (Figure S9.2). These differ in the orientations of the ethylene  $\pi$ -bond that is coordinated to the Ni-center. In **int1-et-c1**, the  $\pi$ -bond is perpendicular to the Ni square plane, whereas in **int1-et-c2**, the  $\pi$ -bond is parallel to and lying on the Ni square plane. Structure **int1-et-c1** is 5.9 kcal mol<sup>-1</sup> more stable than **int1-et-c2**. For the migratory insertion of ethylene substrate into the Ni–C bond, the ethylene has to be in **int1-et-c2** before insertion can occur (*vide infra*).

### 9.1.3 t-butylacrylate (tBA)-bound Ni(II) complex – displacement of pyridine by tBA in **POP-Ni-py**

We similarly show the optimized structures of the Ni(II) complex where the pyridine ligand gets displaced by t-butylacrylate (tBA) substrate. All possibilities were considered while minimizing / avoiding unphysical steric clashes. The optimized structures are given in Figure S9.3. We denote these as **POP-Ni-ac** complexes where the suffix “**ac**” denotes t-butylacrylate.

tBA can coordinate either via the C=C  $\pi$ -bond or the O-atom of the carbonyl group. For the coordination via C=C  $\pi$ -bond to the Ni-center, both the C=C bond perpendicular (**int1-ac-c1** and **int1-ac-c2**) and parallel (**int1-ac-c3** and **int1-ac-c4**) to the Ni square plane can be found. As in the case of ethylene binding, the tBA binding with C=C  $\pi$ -bond perpendicular to the Ni square plane is lower in energy/more stable (by at least 4.4 kcal mol<sup>-1</sup>) than with C=C  $\pi$ -bond parallel to the Ni square plane. Comparing the latter two structures (**int1-ac-c3** and **int1-ac-c4**) which the reaction must pass prior to migratory insertion, we found that **int1-ac-c3**, forming the observed tBA insertion product, is 5.1 kcal mol<sup>-1</sup> more stable than **int1-ac-c4**, which forms the less favorable regioisomer (*vide infra*).

For tBA insertion, additionally, two structures with O-coordination were found (**int1-ac-o1** and **int1-ac-o2**). These differ in the orientation of the *t*-butoxy group. Both these O-coordinated structures have lower energy than C=C  $\pi$ -bond coordinated species (by 2.2 kcal mol<sup>-1</sup> comparing the lowest energy coordination species, **int1-ac-o1** and **int1-ac-c1**), suggesting that the initial coordination of tBA substrate would occur via O-coordination.

Coordination via C=C $\pi$ -bond	
<b>int1-ac-c1</b>	<b>int1-ac-c2</b>
$\Delta G = 13.7$	$\Delta G = 15.6$
	
<b>int1-ac-c3</b>	<b>int1-ac-c4</b>
$\Delta G = 20.0$	$\Delta G = 25.1$

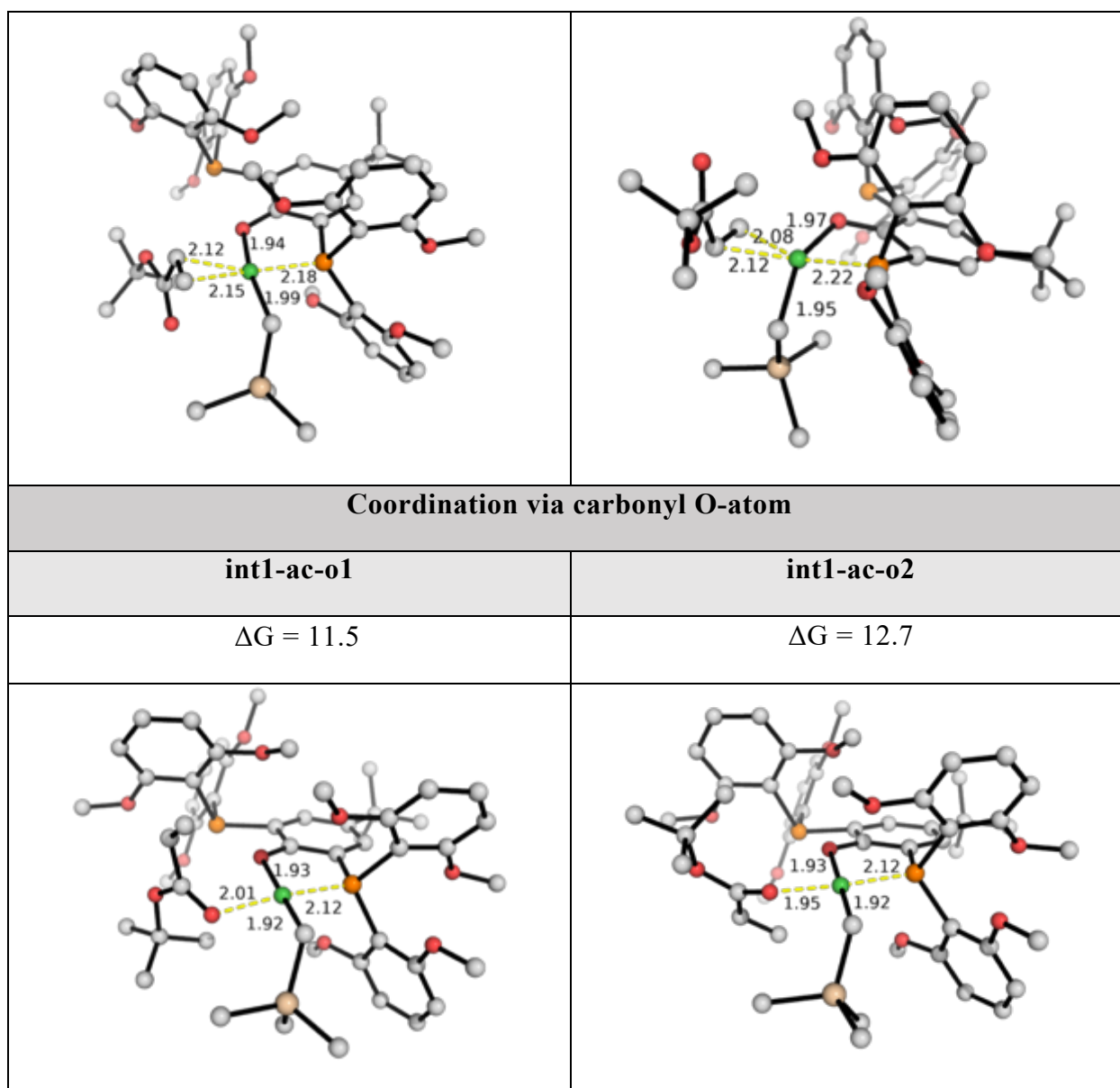


**Figure S9.3.** Optimized structures for the Ni(II) complex **POP-Ni-ac**. The Gibbs energies are calculated relative to **POP-Ni-py (1)**. Key bond distances are given in Å. Gibbs energy units are given in kcal mol<sup>-1</sup>.

#### 9.1.4 First insertion of substrate into POP-Ni-py (1)

We investigated the comparative barriers of the insertion of ethylene vs tBA into catalyst **POP-Ni-py (1)**. Figure S9.4 shows the reaction scheme and the Gibbs energy profile for the first insertion. The optimized TS structures and their key bond distances are given in Figure S9.5. From this energy profile, we can see that the 2,1-insertion of acrylate tBA (**ts1-ac**, at 30.5 kcal mol<sup>-1</sup>) has a lower activation barrier, by 2.6 kcal mol<sup>-1</sup>, at the reaction temperature

of 50 °C, than the insertion of ethylene (**ts1-et**, at 33.1 kcal mol<sup>-1</sup>); the regioisomeric 1,2-insertion of tBA (**ts1-ac-r**) is the least favorable, with a barrier of 41.5 kcal mol<sup>-1</sup>. Comparing the migratory insertion site selectivity of tBA (2,1-insertion vs 1,2-insertion), our calculation is in agreement with the observation that the migratory insertion of acrylate occurs at the  $\beta$ -carbon site of an  $\alpha,\beta$ -unsaturated carbonyl, akin to conjugate addition.<sup>29-31</sup> Using simple transition state theory (TST), this translates to a rate of roughly **ts1-ac** : **ts1-et** : **ts1-ac-r** = 1 : 57 : 27 million. With this energy profile, it implicates that the insertion of acrylate can occur more easily than the insertion of ethylene, which is contradictory to the experimental observation that the first insertion of ethylene proceeds *ca.* 50 times faster than the tBA insertion. In addition, the overall barriers of 30.5 kcal mol<sup>-1</sup> for tBA insertion and 33.1 kcal mol<sup>-1</sup> for ethylene insertion seem pretty high. We anticipate that the Ni-catalyst **POP-Ni-py (1)** can undergo an isomerization before subsequent first insertion occurs, giving a lower activation barrier and correct substrate selectivity (see section 7.2).



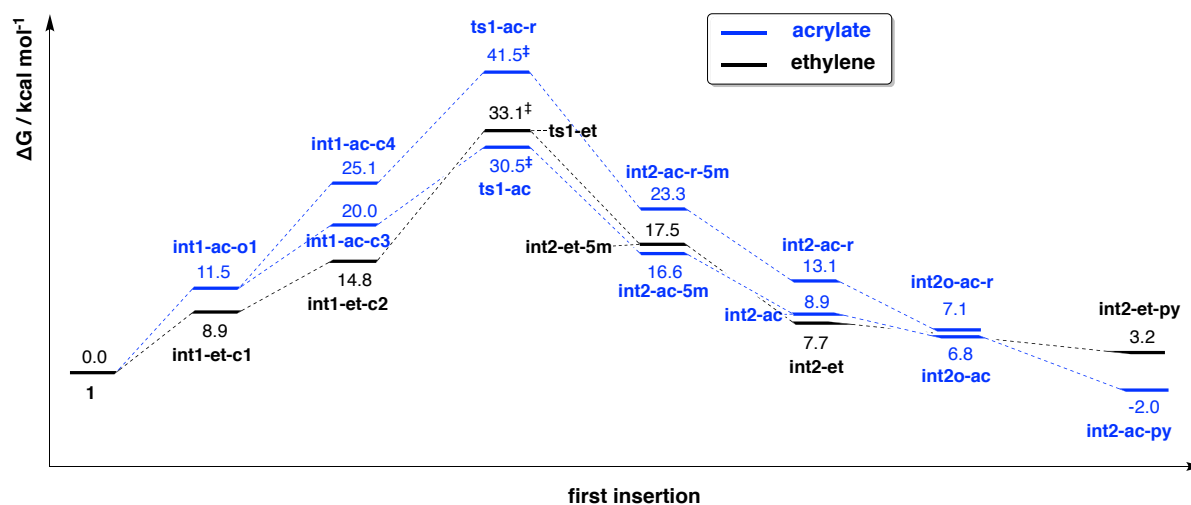
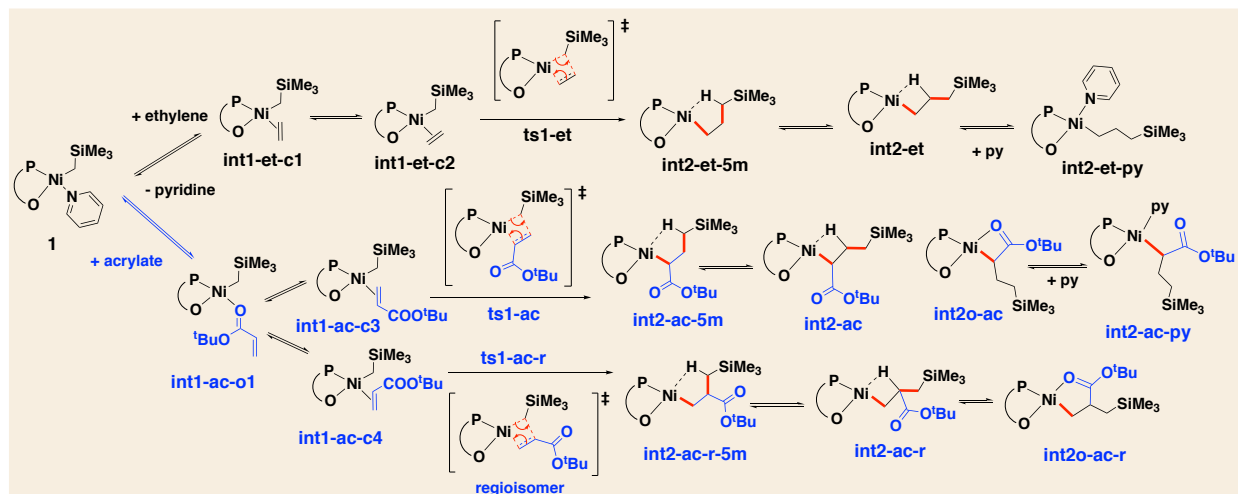


**Figure S9.4.** Gibbs energy profile for the first insertion of ethylene vs *t*-butylacrylate into catalyst **POP-Ni-py (1)**. The Gibbs energies are calculated at SMD(chlorobenzene)-M06/def2-TZVP//M06/def2-SVP level of theory. The Gibbs energy of the species **POP-Ni-py (1)** is taken as a reference.

The first insertion products have the  $\beta$ -H atom coordinated to the Ni-center, forming 4-membered nickelacycles (**int2-et**, **int2-ac** and **int2-ac-r**). These 4-m nickelacycles are lower in energy than the 5-m nickelacycles formed via  $\gamma$ -H atom coordination (**int2-et-5m**, **int2-ac-5m** and **int2-ac-r-5m**), as located by IRC analysis.

ts1-et	ts1-ac
$\Delta G^\ddagger = 33.1$	$\Delta G^\ddagger = 30.5$

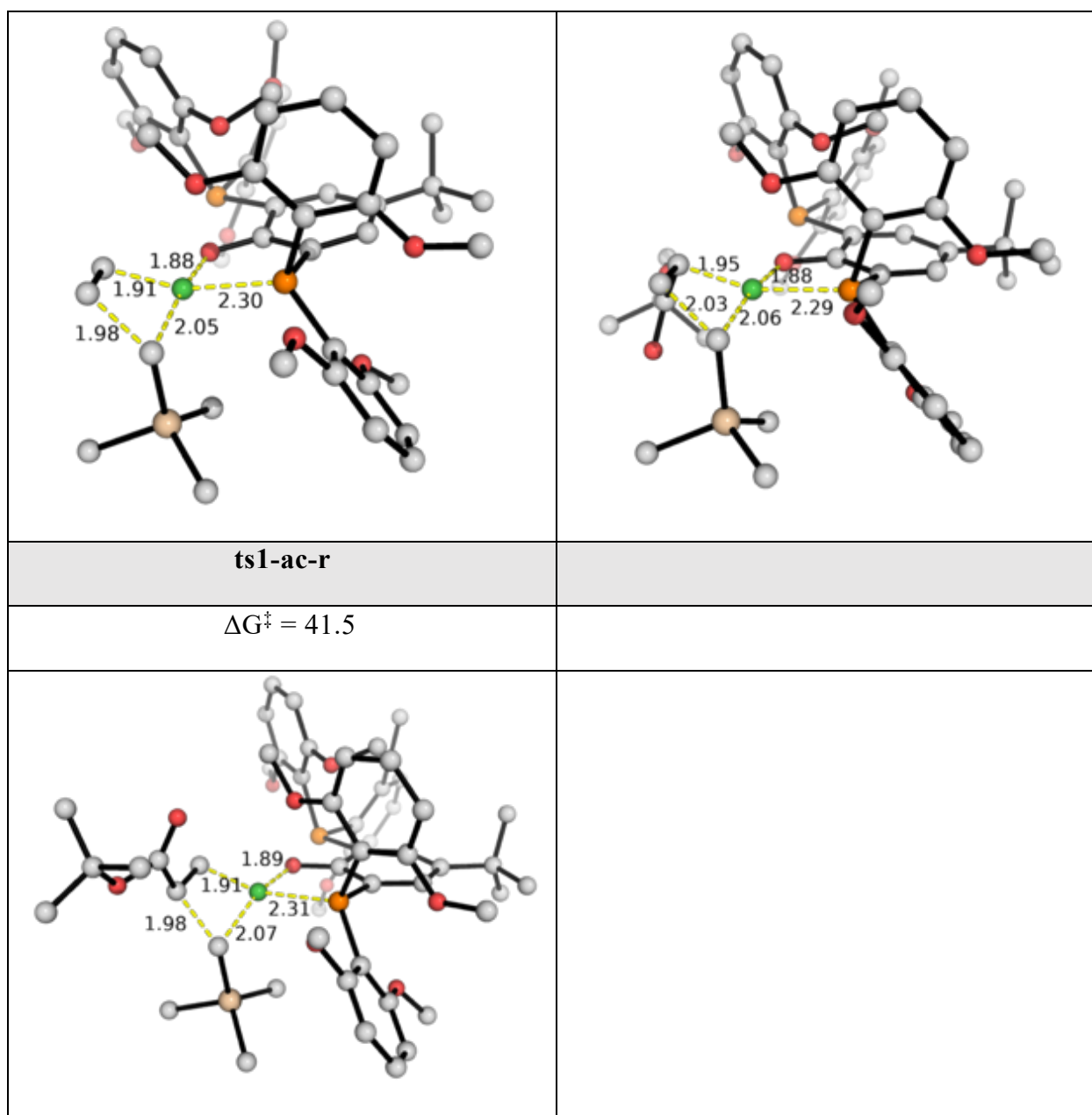
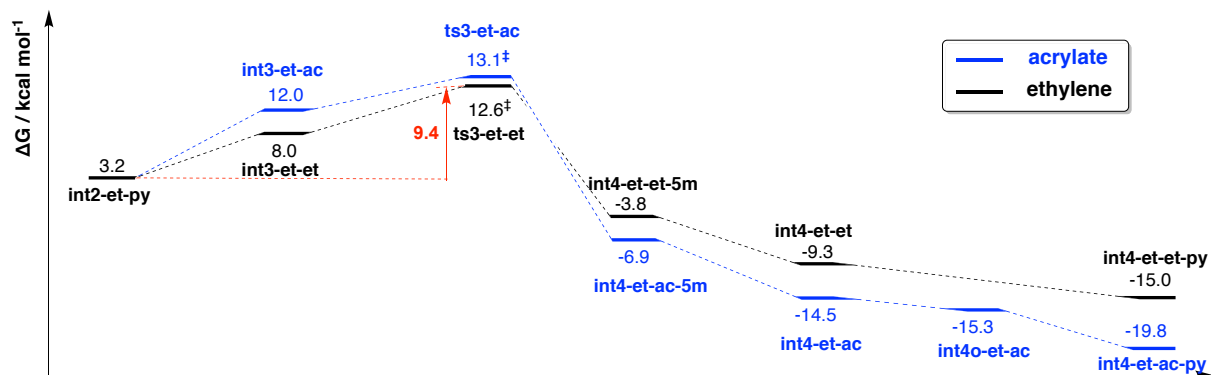
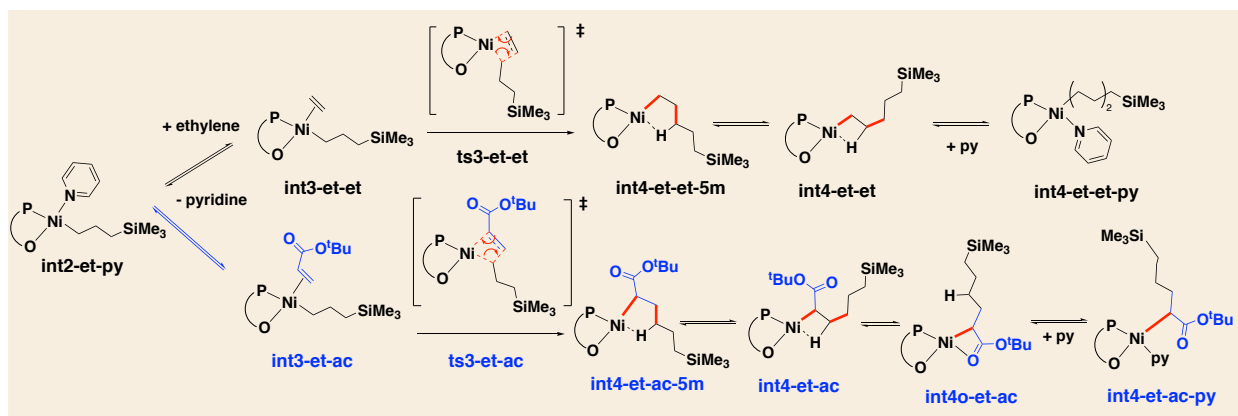


**Figure S9.5.** Optimized TS structures of first insertion of ethylene/tBA into Ni(II) complex **POP-Ni-ac 1**. Key bond distances are given in Å. Gibbs energy units are given in kcal mol<sup>-1</sup>.

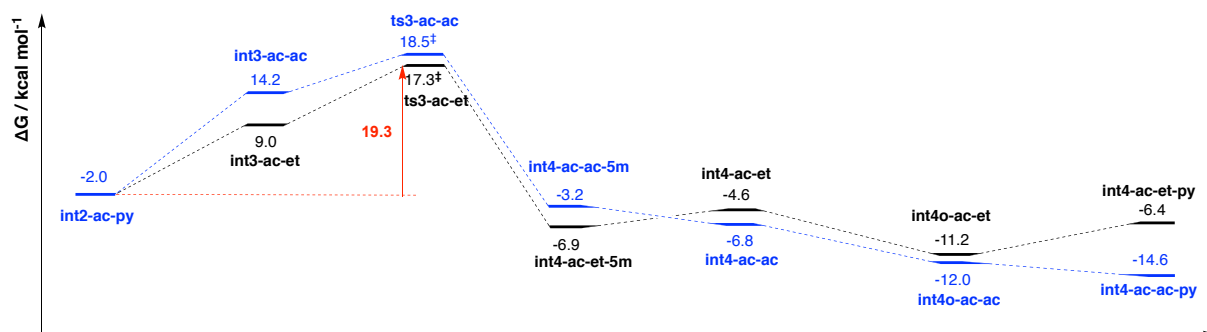
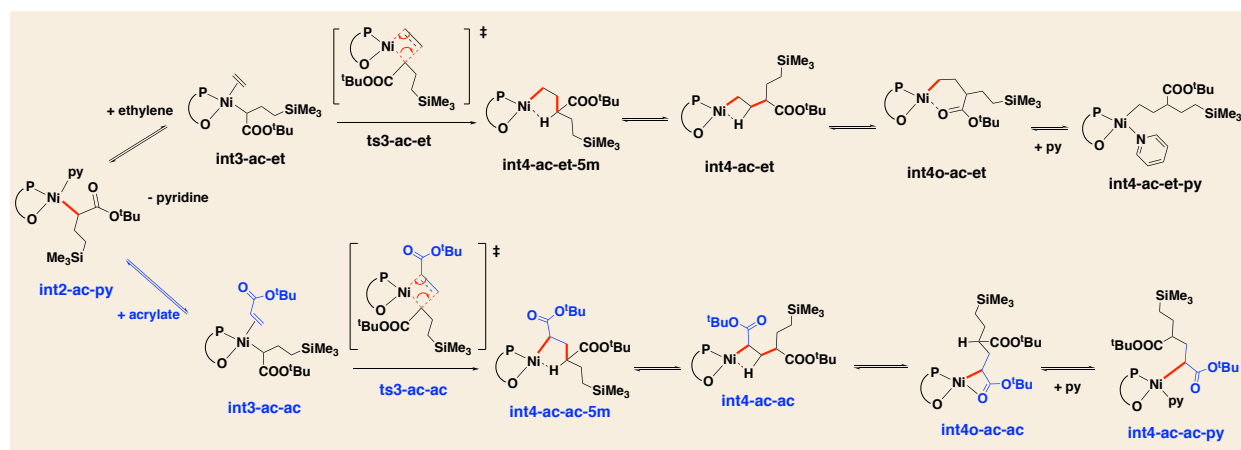
### 9.1.5 Second insertion of monomer into first insertion product of POP-Ni-py (1)

The insertion of second monomer after the first insertion of ethylene vs tBA into catalyst **POP-Ni-py 1** was studied. Figure S9.6 presents the Gibbs energy profile for the second insertion; optimized TS structures are given in Figure S9.7. In Figure S9.6 (a), we see that the second insertion of ethylene to first ethylene-inserted product has a rather low activation barrier of 9.4 kcal mol<sup>-1</sup> (**ts3-et-et**, at 12.6 kcal mol<sup>-1</sup>). The second insertion of tBA into first

ethylene-inserted product has a slightly higher activation barrier, by 0.5 kcal mol<sup>-1</sup> (**ts3-et-ac**, at 13.1 kcal mol<sup>-1</sup>). This energetic difference is rather small and typically falls within the numerical accuracy of DFT. This implies that the rate of second insertion of ethylene would be rather similar to that of acrylate into first ethylene-inserted product. The insertion products having 4-membered nickelacycles via  $\beta$ -H agostic interaction with the Ni-center (**int4-et-et** and **int4-et-ac**) have lower energies than the 5-membered nickelacycles formed via  $\gamma$ -H atom coordination (**int4-et-et-5m** and **int4-et-ac-5m**), as located by IRC analysis. We note that, however, these energetic differences do not affect the overall conclusion of the kinetic analyses as these species are not involved in turnover-frequency determining steps.

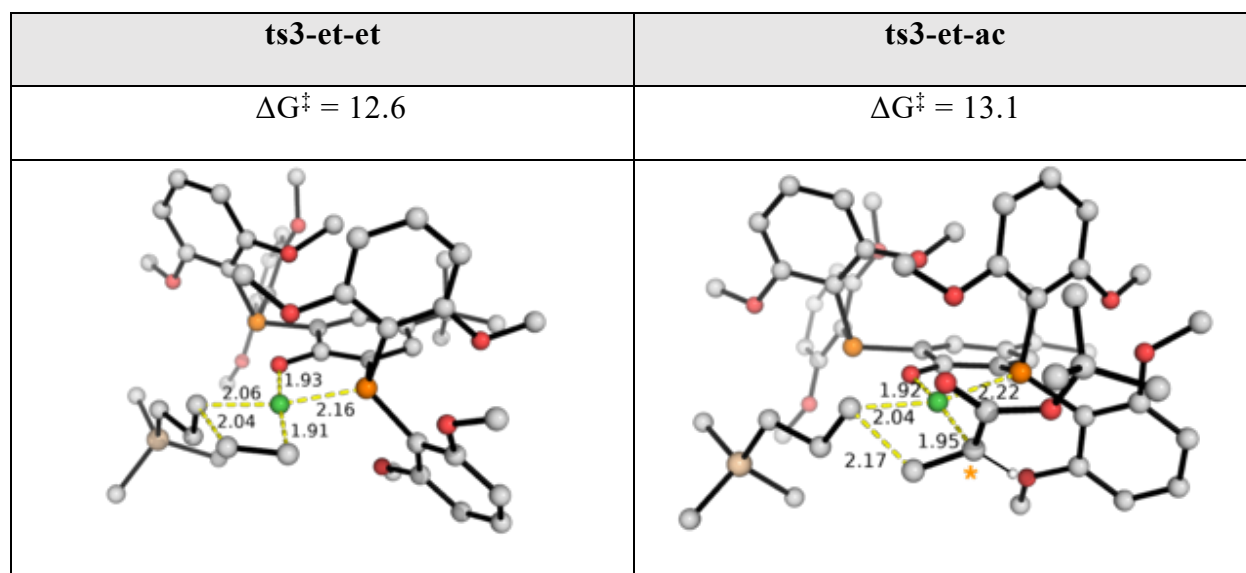


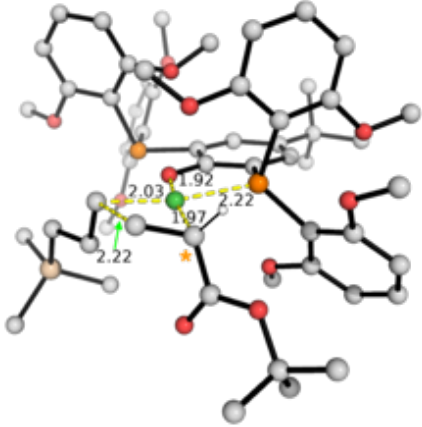
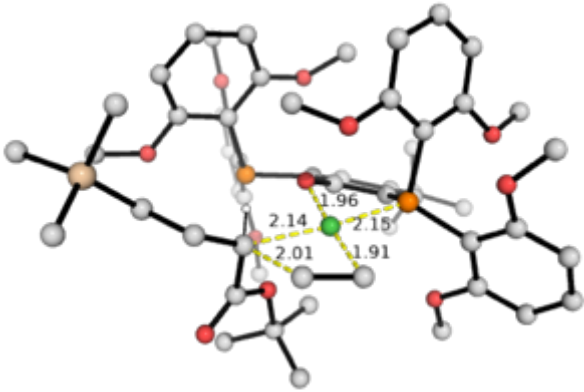
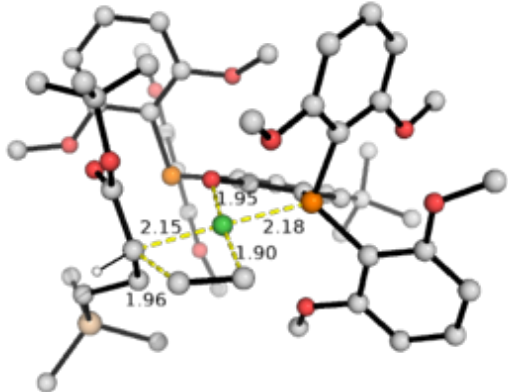
(a) second insertion after first ethylene insertion



(b) second insertion after first acrylate insertion

**Figure S9.6.** Gibbs energy profile for the second insertion of ethylene vs *t*-butylacrylate into first inserted product resulting from catalyst **POP-Ni-py** (**1**). The energy of the species **POP-Ni-py** (**1**) is taken as a reference. (a) Second insertion after first ethylene insertion product and (b) second insertion after first acrylate insertion product.



<b>ts3-et-ac-c2</b>	
$\Delta G^\ddagger = 14.0$	
	
<b>ts3-ac-et</b>	<b>ts3-ac-et-c2</b>
$\Delta G^\ddagger = 17.3$	$\Delta G^\ddagger = 26.9$
	
<b>ts3-ac-ac</b>	<b>ts3-ac-ac-c2</b>
$\Delta G^\ddagger = 18.5$	$\Delta G^\ddagger = 18.5$

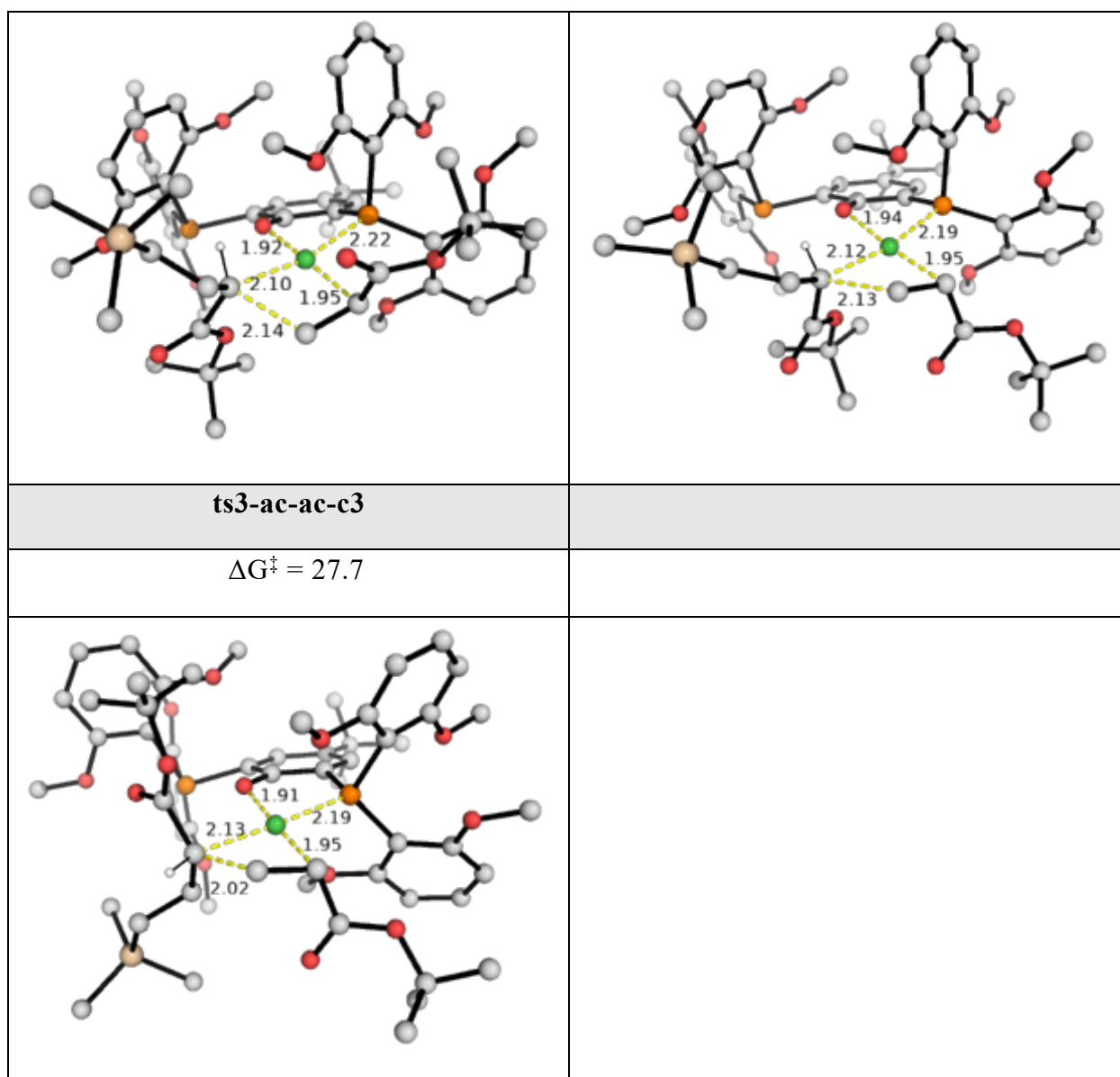


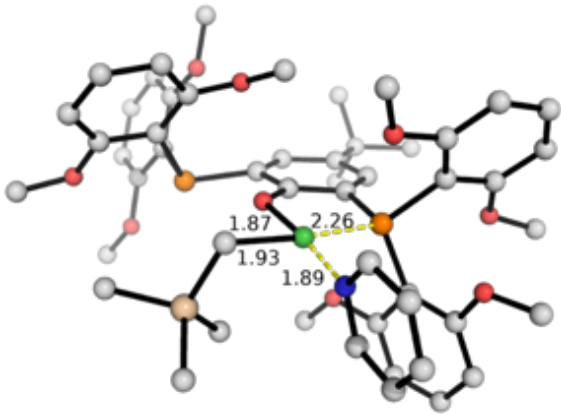
**Figure S9.7.** Optimized TS structures of second insertion of ethylene/tBA into first inserted product arising from Ni(II) complex POP-Ni-ac **1**. Key bond distances are given in Å. Gibbs energy units are given in kcal mol<sup>-1</sup>.

For the second insertion of monomer into first acrylate-inserted product (Figure S9.6 (b)), the insertion of ethylene (**ts3-ac-et**, at 17.3 kcal mol<sup>-1</sup>) has a barrier that is 1.2 kcal mol<sup>-1</sup> lower than the second insertion of tBA (**ts3-ac-ac**, at 18.5 kcal mol<sup>-1</sup>). The overall barrier for the second insertion into tBA-inserted product (28.9 kcal mol<sup>-1</sup>) is much higher than the overall barrier for the second insertion into ethylene-inserted (9.4 kcal mol<sup>-1</sup>), suggesting that the second insertion into acrylate-inserted product will be much more difficult than the second insertion into ethylene-inserted product.

## 9.2 Reaction pathways leading from the geometric isomer of the catalyst POP-Ni-py (1')

### 9.2.1 Geometric isomer POP-Ni-py (1') and its relevant substrate-bound complexes

Previous report by Morokuma and Nozaki on Pd phosphine-sulfonate-catalyzed polymerization<sup>31</sup> suggests that the olefin can insert to the growing polymer chain that is *trans* to the phosphorus atom. We herein consider the insertion to the geometric isomeric form of the **POP-Ni-py** catalyst, denoted as **1'**. The optimized structures of this pyridine-bound catalyst and the relevant substrate-bound complexes are shown in Figure S9.8. The relative energies are given with respect to the most stable form **POP-Ni-py 1**.

<b>1'</b>	
$\Delta G = 4.4$	
	
<b>Coordination of ethylene via C=C <math>\pi</math>-bond</b>	
<b>int1'-et-c1</b>	<b>int1'-et-c2</b>
$\Delta G = 11.7$	$\Delta G = 14.6$

<b>Coordination of tBA via C=C <math>\pi</math>-bond</b>	
<b>int1'-ac-c1</b>	<b>int1'-ac-c2</b>
$\Delta G = 14.7$	$\Delta G = 18.4$
<b>int1'-ac-c3</b>	<b>int1'-ac-c4</b>
$\Delta G = 19.4$	$\Delta G = 20.6$



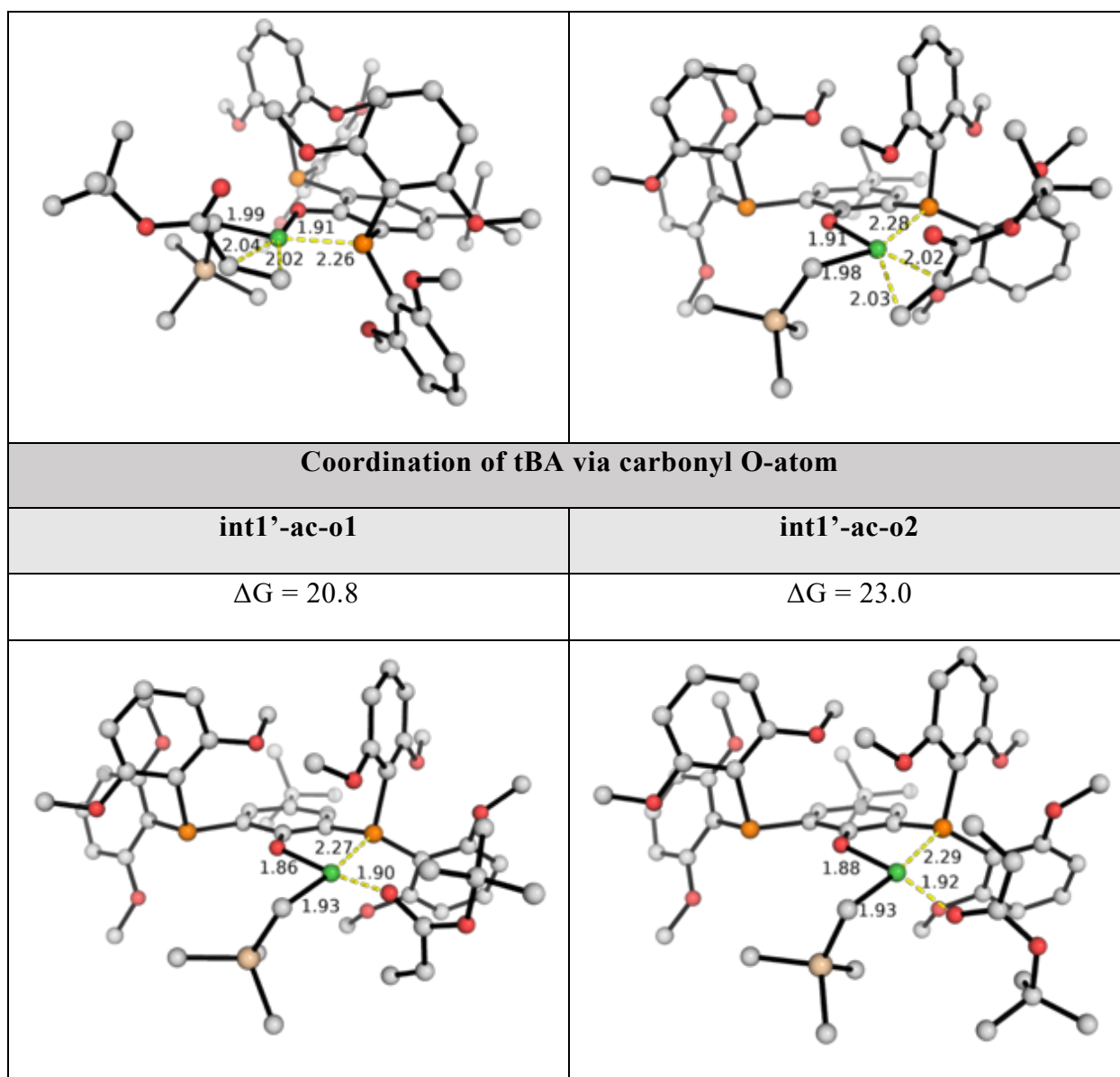
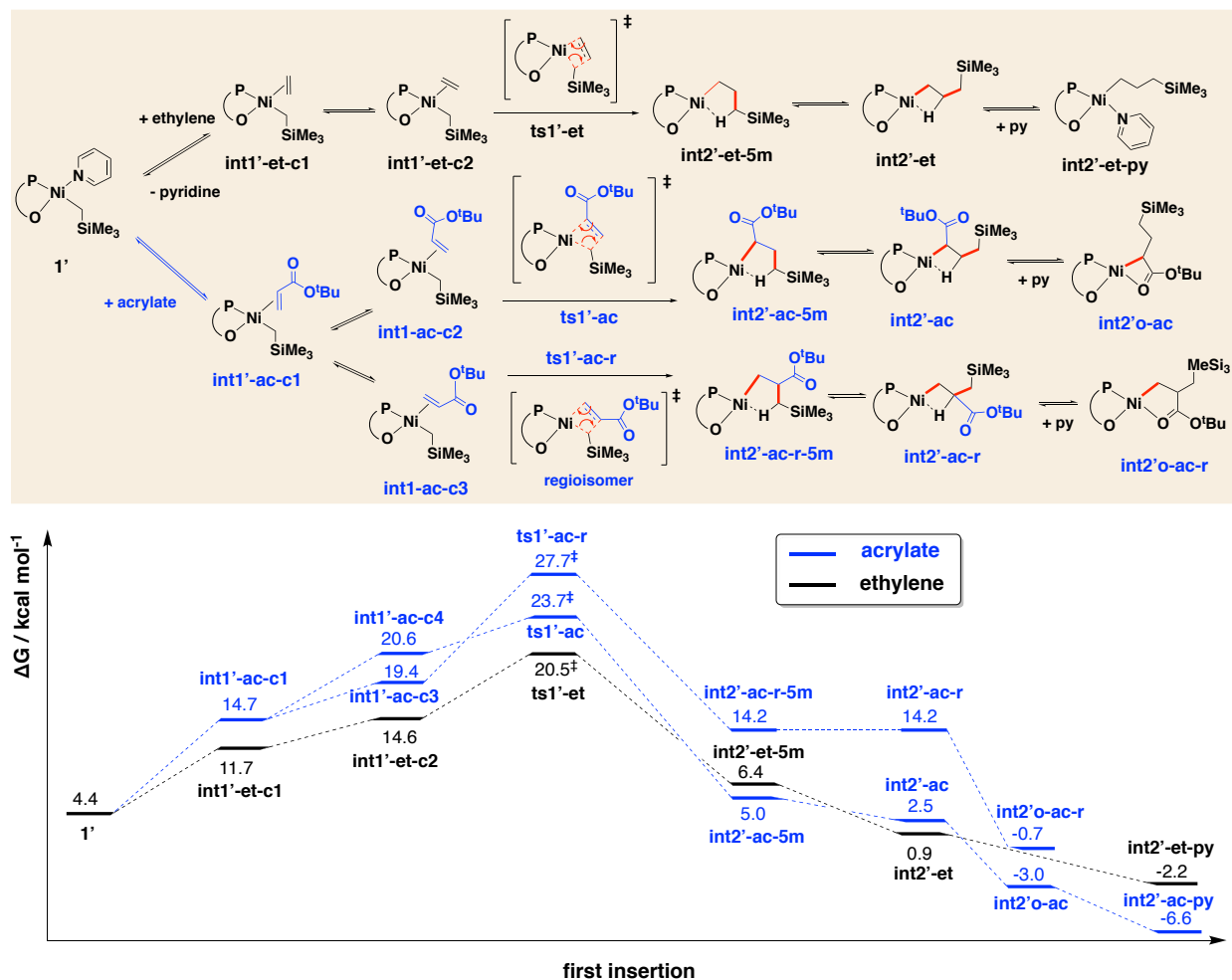


**Figure S9.8.** Optimized structures for the coordination complexes of the isomeric Ni-catalyst **1**<sup>†</sup>. The Gibbs energies are calculated relative to **POP-Ni-py (1)**. Key bond distances are given in Å. Gibbs energy units are given in kcal mol<sup>-1</sup>.

It is interesting to note here that, for the coordination complex with tBA monomer, the coordination via  $\pi_{CC}$  bond (**int1'-ac-c1**, at 14.7 kcal mol<sup>-1</sup>) is much more stable, by 6.1 kcal mol<sup>-1</sup>, than the coordination via oxygen atom (**int1'-ac-o1**, at 20.8 kcal mol<sup>-1</sup>) (cf Figure S9.3). This difference possibly arises due to the electronic differences at Ni-metal relative to the ligand coordination from phenoxy-O and phosphine-P atoms. Herein the  $\pi$  donation is more favored than lone pair donation *cis* to P-atom, compared to the other way when tBA coordinates *trans* to P-atom (Figure S9.3).

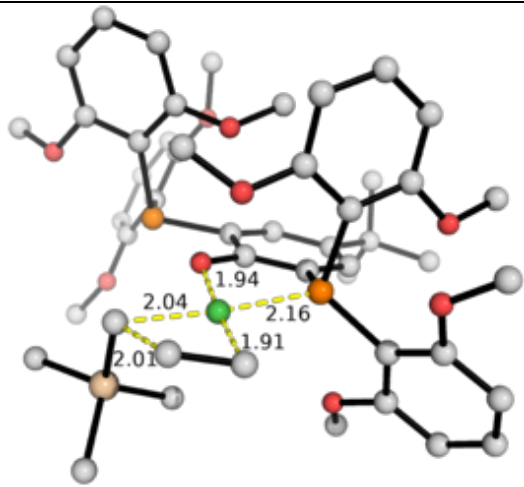
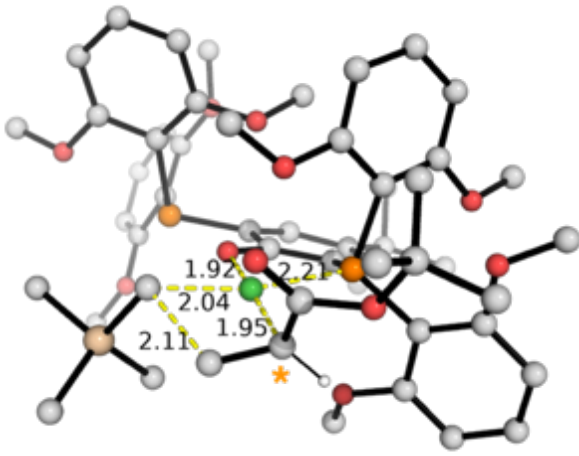
### 9.2.3 First insertion of substrate into isomeric POP-Ni-py (1')

The insertion of ethylene vs tBA into isomeric **POP-Ni-py 1'** was calculated. The Gibbs energy profile is shown in Figure S9.9 and the optimized TS structures are given in Figure S9.10. All values are given in kcal mol<sup>-1</sup> and take the energy of the catalyst **POP-Ni-py 1** as a reference. From this energy profile, we can see that the insertion of ethylene into the isomeric form of the Ni-catalyst has the lowest activation barrier (**ts1'-et**, at 20.5 kcal mol<sup>-1</sup>). The insertion of tBA in either ways (**ts1'-ac**, at 23.7 kcal mol<sup>-1</sup> and **ts1'-ac-r**, at 27.7 kcal mol<sup>-1</sup>) are both less favorable. In particular, the insertion of ethylene is 3.2 kcal mol<sup>-1</sup> more favorable than the 2,1-insertion of tBA, translating to a selectivity in favor of ethylene insertion by about 146 folds using simple TST.



**Figure S9.9.** Gibbs energy profile for the first insertion of ethylene vs *t*-butylacrylate into isomeric form of the Ni-catalyst POP-Ni-py (**1'**). The Gibbs energies are calculated at SMD(chlorobenzene)-M06/def2-TZVP//M06/def2-SVP level of theory. The energy of the species POP-Ni-py (**1**) is taken as a reference

More importantly, the overall barrier of 20.5 kcal mol<sup>-1</sup> for ethylene insertion (taking the most stable catalyst **1** as the energy reference, assuming that the geometric isomers **1** and **1'** can interconvert rather easily) is much lower (by at least 10 kcal mol<sup>-1</sup>) than the activation barriers observed for the insertion into catalyst **1** (Figure S9.4). In other words, if the isomerization of **1** to **1'** can occur easily (*vide infra*), then the insertion of ethylene will occur through the isomeric form of the catalyst via **ts1'-et**. This is in agreement with prior DFT studies of Pd-catalyzed ethylene polymerization<sup>24</sup> where the migratory insertion of the growing polymer chain can occur more readily when it is *trans* to P-atom (*trans* effect).

<b>ts1'-et</b>	<b>ts1'-ac</b>
$\Delta G^\ddagger = 20.5$	$\Delta G^\ddagger = 23.7$
	
<b>ts1'-ac-c2</b>	<b>ts1'-ac-r</b>
$\Delta G^\ddagger = 24.2$	$\Delta G^\ddagger = 27.7$

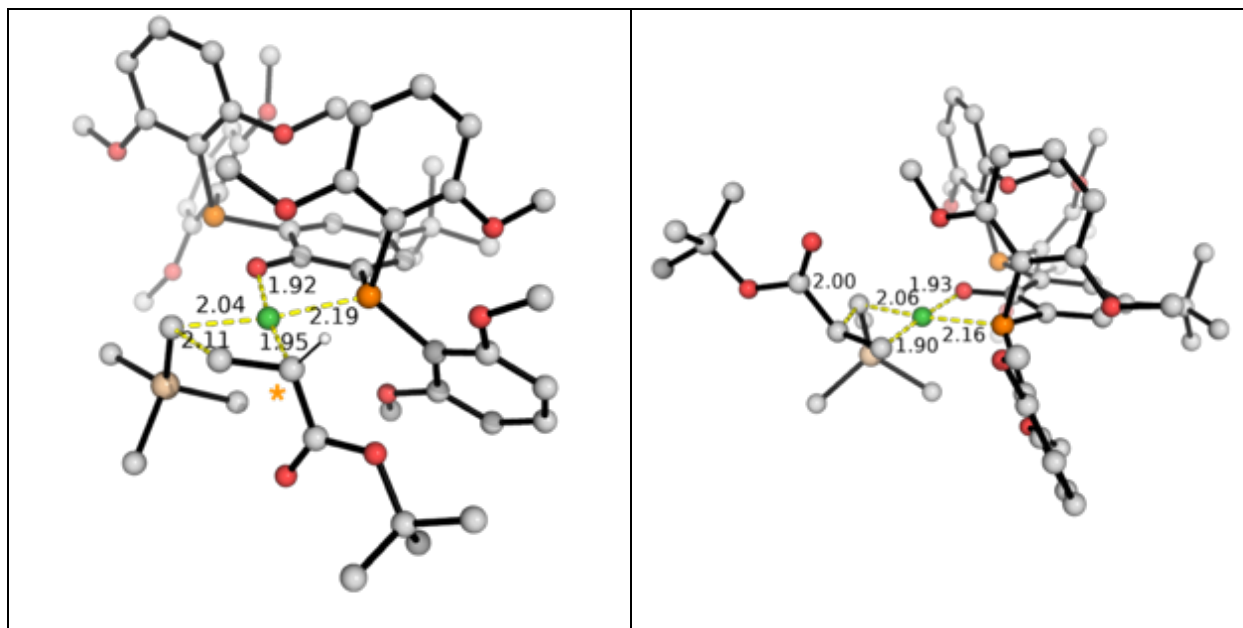


**Figure S9.10.** Optimized structures for the TS structures of first insertion of ethylene/tBA into Ni(II) complex **POP-Ni-ac 1**. Stereocenters in **ts1'-ac** and **ts1'-ac-c2** are marked with yellow asterisk (\*). Key bond distances are given in Å. Gibbs energy units are given in kcal mol<sup>-1</sup>.

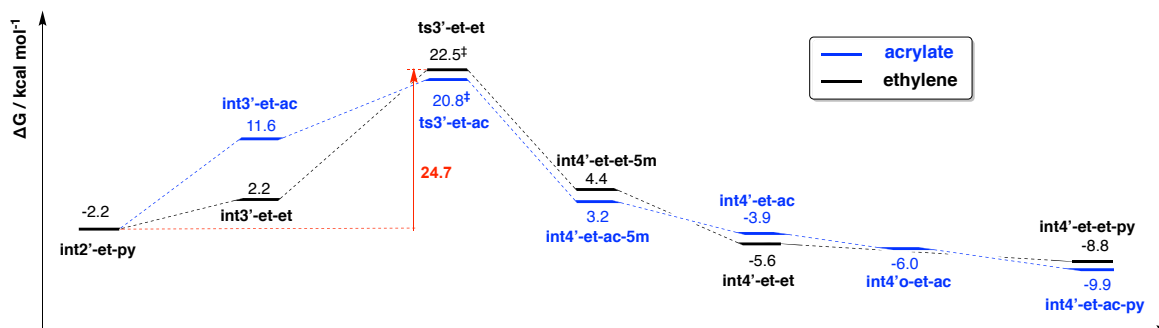
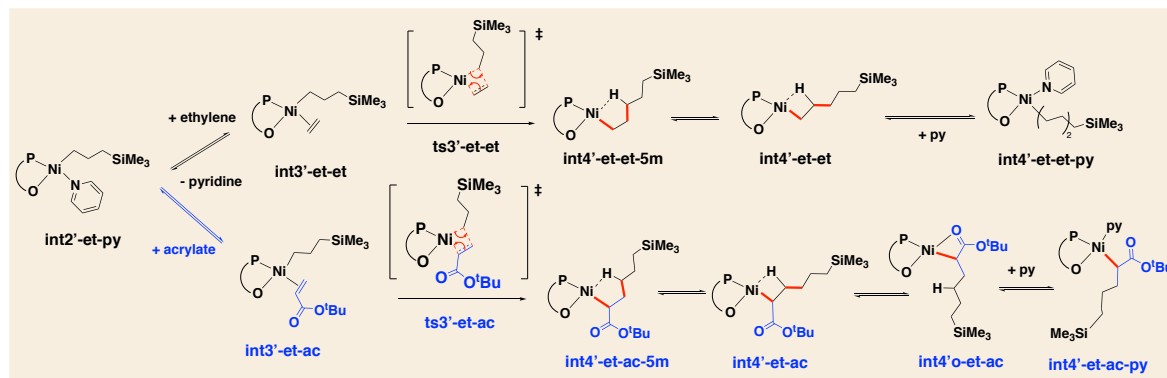
Comparing the migratory insertion site selectivity of tBA, herein the migratory insertion of acrylate occurs more readily, by 4.0 kcal mol<sup>-1</sup>, at the β-carbon site of the α,β-unsaturated carbonyl (**ts1'-ac**, at 23.7 kcal mol<sup>-1</sup>) than at the α-carbon site (**ts1'-ac-r**, at 27.7 kcal mol<sup>-1</sup>), as previously. For the migratory insertion at the β-carbon, two possibilities can occur (**ts1'-ac** and **ts1'-ac-c2**), giving a stereocenter at the α-carbon (Figure S9.10). We took the lowest TS for all subsequent second insertion.

### 9.2.3 Second insertion of monomer into first insertion product of isomeric POP-Ni-py (1')

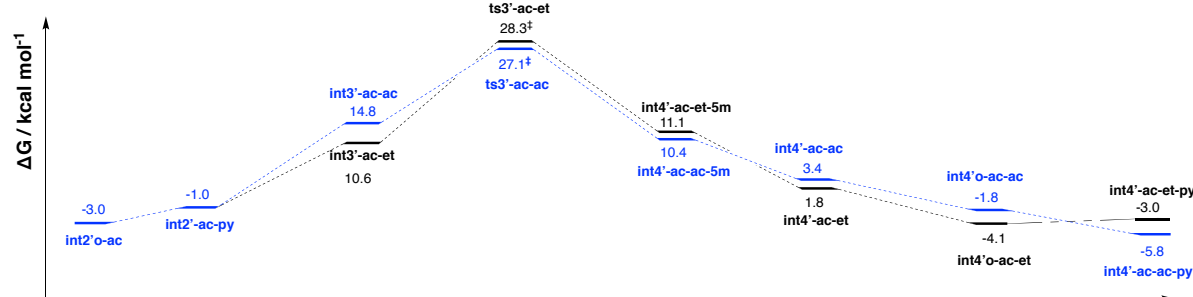
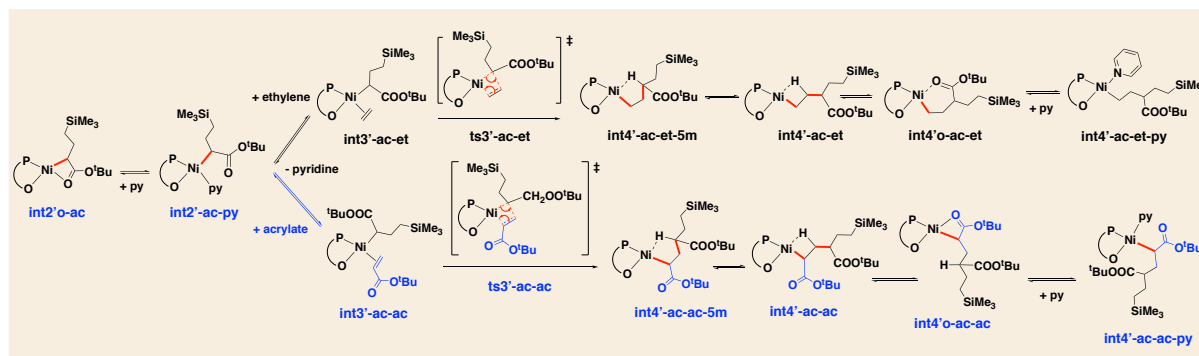
The insertion of second monomer after the first insertion of ethylene vs tBA into the geometric isomeric catalyst **POP-Ni-py 1'** was studied. Figure S9.11 presents the Gibbs energy profile for the second insertion and Figure S9.12 gives the optimized TS structures. In Figure S9.11 (a), we can see that the second insertion of ethylene to first ethylene-inserted product has a slightly higher barrier, by 1.7 kcal mol<sup>-1</sup> (**ts3'-et-et**, at 22.5 kcal mol<sup>-1</sup>) than the second insertion of acrylate tBA into first ethylene-inserted product (**ts3'-et-ac**, at 20.8 kcal mol<sup>-1</sup>).

This implies that the second insertion of tBA is predicted to occur more rapidly via this pathway, which is inconsistent with experimental observation that the second insertion of ethylene after first ethylene insertion occurs more rapidly than the second insertion of tBA. We note that, similar to first insertion, these second insertions where the growing chain originate from Ni-coordination site *cis* to the P-atom of the ligand have higher activation barriers than the corresponding second insertions where the growing polymer chain is *trans* to the P-atom (Figure S9.6 (a)). Again, we hypothesize that the initial catalyst **1** having growing polymer chain *cis* to the P-atom of the ligand can isomerize to its geometric isomer **1'** where the growing polymer chain is *trans* to the P-atom of the ligand before first insertion occurs (Figure S9.9). The ethylene insertion product **int2'-et-py** at  $-2.2 \text{ kcal mol}^{-1}$  can undergo another isomerization to **int2-et-py**, at  $3.2 \text{ kcal mol}^{-1}$  before the second insertion of ethylene occurs. The isomerization serves to place the growing polymer chain *trans* to the P-atom of the ligand so that it can take advantage of the *trans* effect of the ligand, making the migratory insertion step easier to occur.

In the second insertion of monomer into the first acrylate-inserted product (Figure S9.11 (b)), we note that the insertion of tBA again has a lower barrier (**ts3'-ac-ac**, at  $27.1 \text{ kcal mol}^{-1}$ ), by  $1.2 \text{ kcal mol}^{-1}$ , than the insertion of ethylene (**ts3'-ac-et**, at  $28.3 \text{ kcal mol}^{-1}$ ), similar to that observed for the second insertion into first ethylene-inserted product in Figure S9.11 (a). This TS for the tBA insertion into tBA-inserted product (**ts3'-ac-ac**, activation barrier of  $30.1 \text{ kcal mol}^{-1}$ ) has a very close activation barrier to TS **ts3-ac-ac** with an activation barrier of  $29.7 \text{ kcal mol}^{-1}$  (Figure S9.6 (b)).

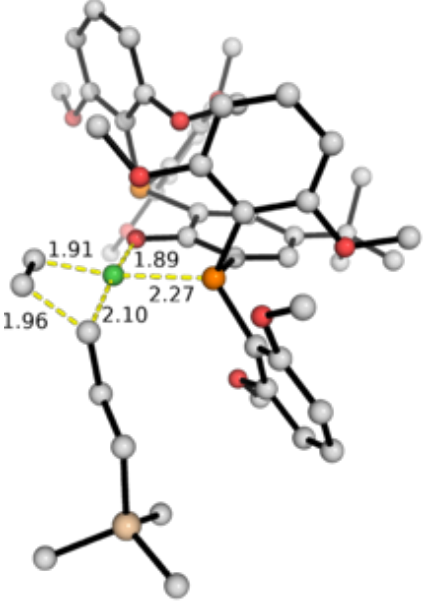
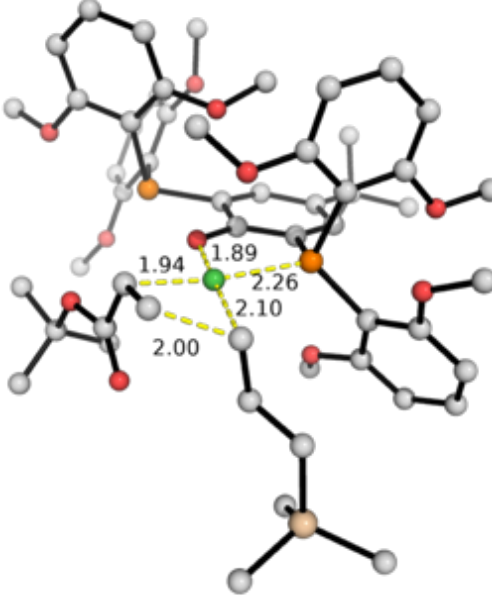
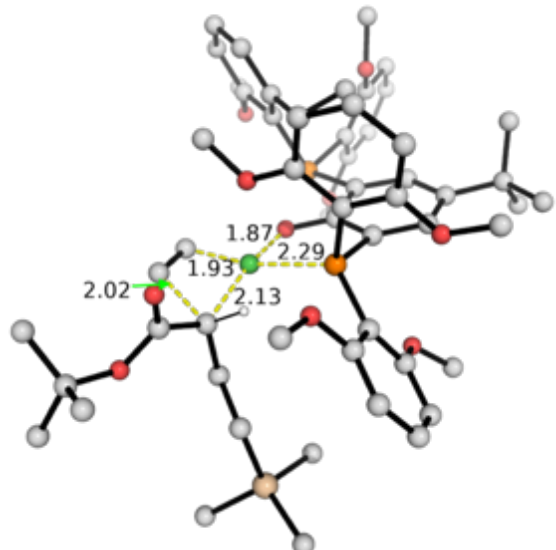
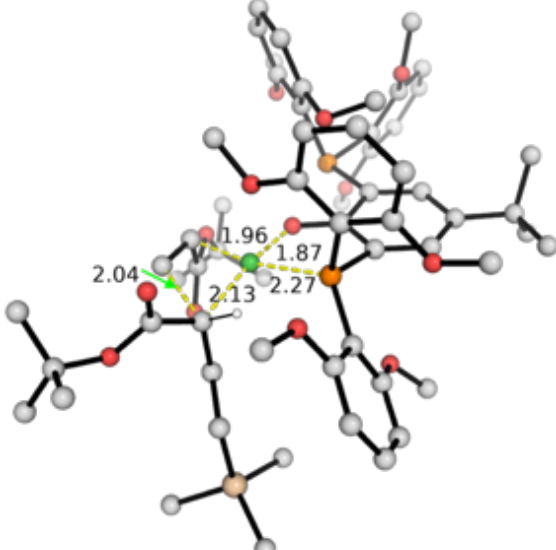


(a) second insertion after first ethylene insertion



(b) second insertion after first acrylate insertion

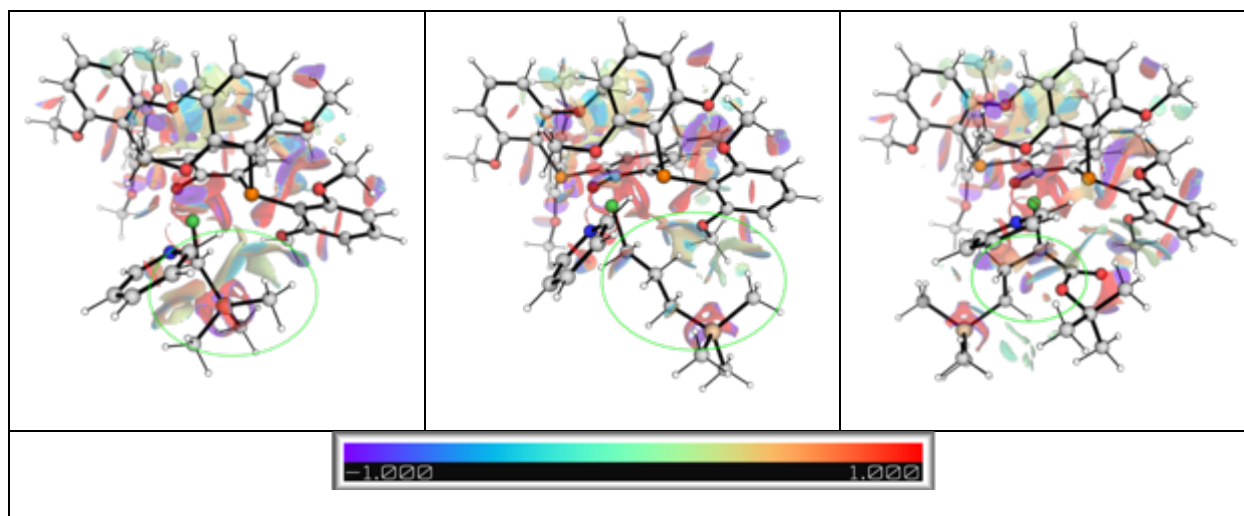
**Figure S9.11.** Gibbs energy profile for the second insertion of ethylene vs *t*-butylacrylate into first inserted product resulting from isomeric catalyst **POP-Ni-py 1'**. The Gibbs energies are calculated at SMD(chlorobenzene)-M06/def2-TZVP//M06/def2-SVP level of theory. The energy of the species **POP-Ni-py (1)** is taken as a reference. **(a)** Second insertion after first ethylene insertion product and **(b)** second insertion after first acrylate insertion product.

ts3'-et-et	ts3'-et-ac
$\Delta G = 22.5$	$\Delta G = 20.8$
	
ts3'-ac-et	ts3'-ac-ac
$\Delta G = 28.3$	$\Delta G = 27.1$
	

**Figure S9.12.** Optimized TS structures of second insertion of ethylene/tBA into first inserted product arising from isomeric Ni(II) complex **POP-Ni-ac 1'**. Key bond distances are given in Å. Gibbs energy units are given in kcal mol<sup>-1</sup>.

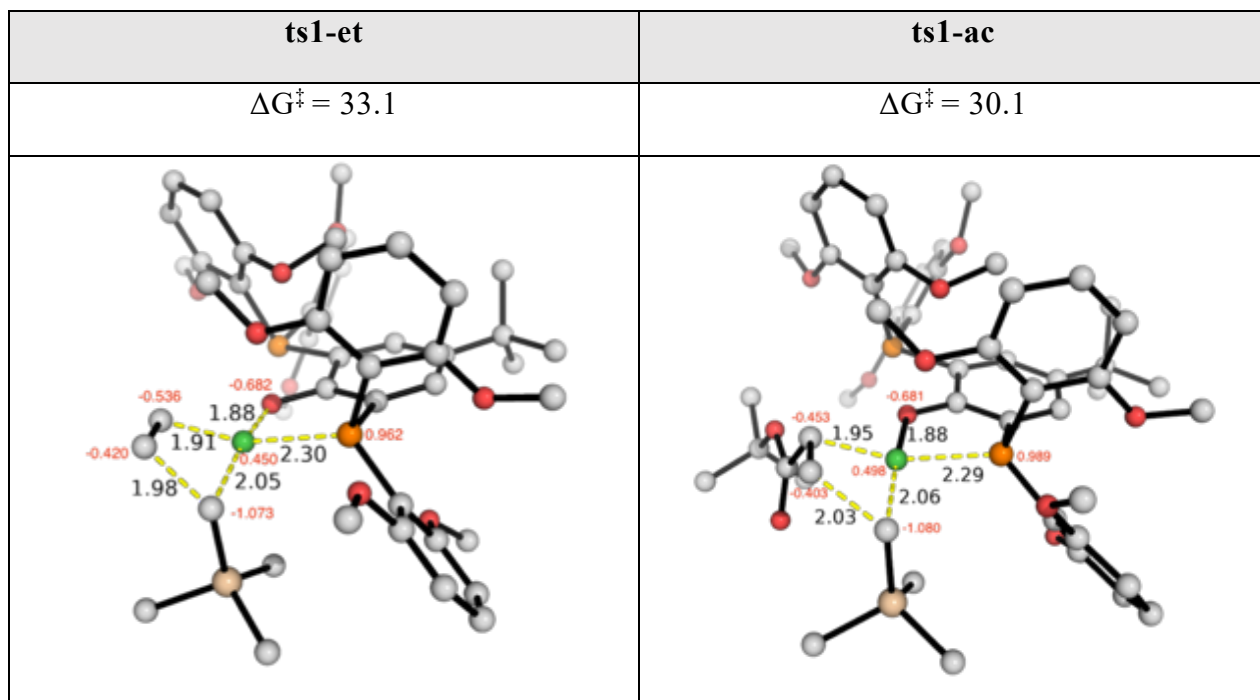


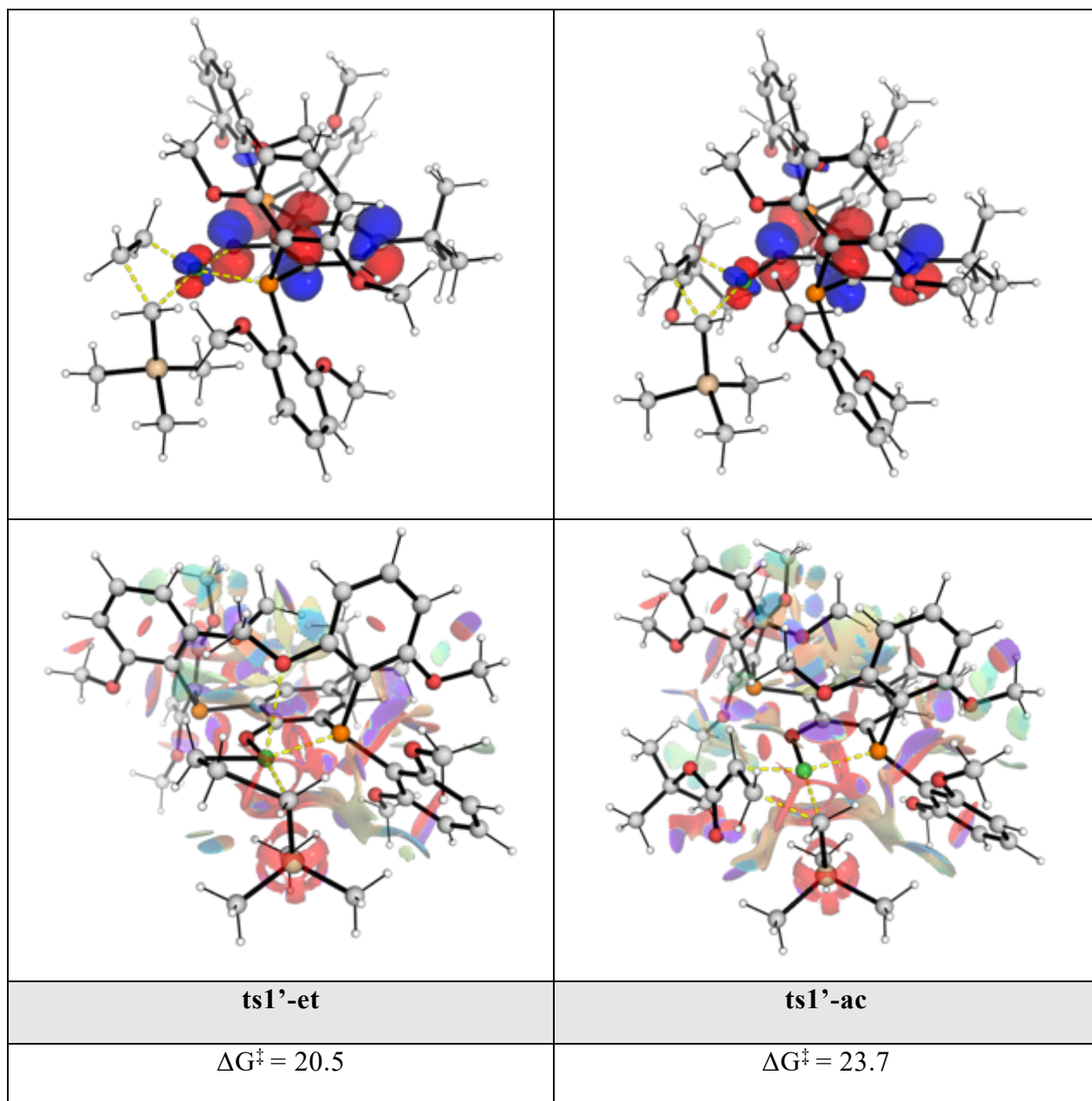


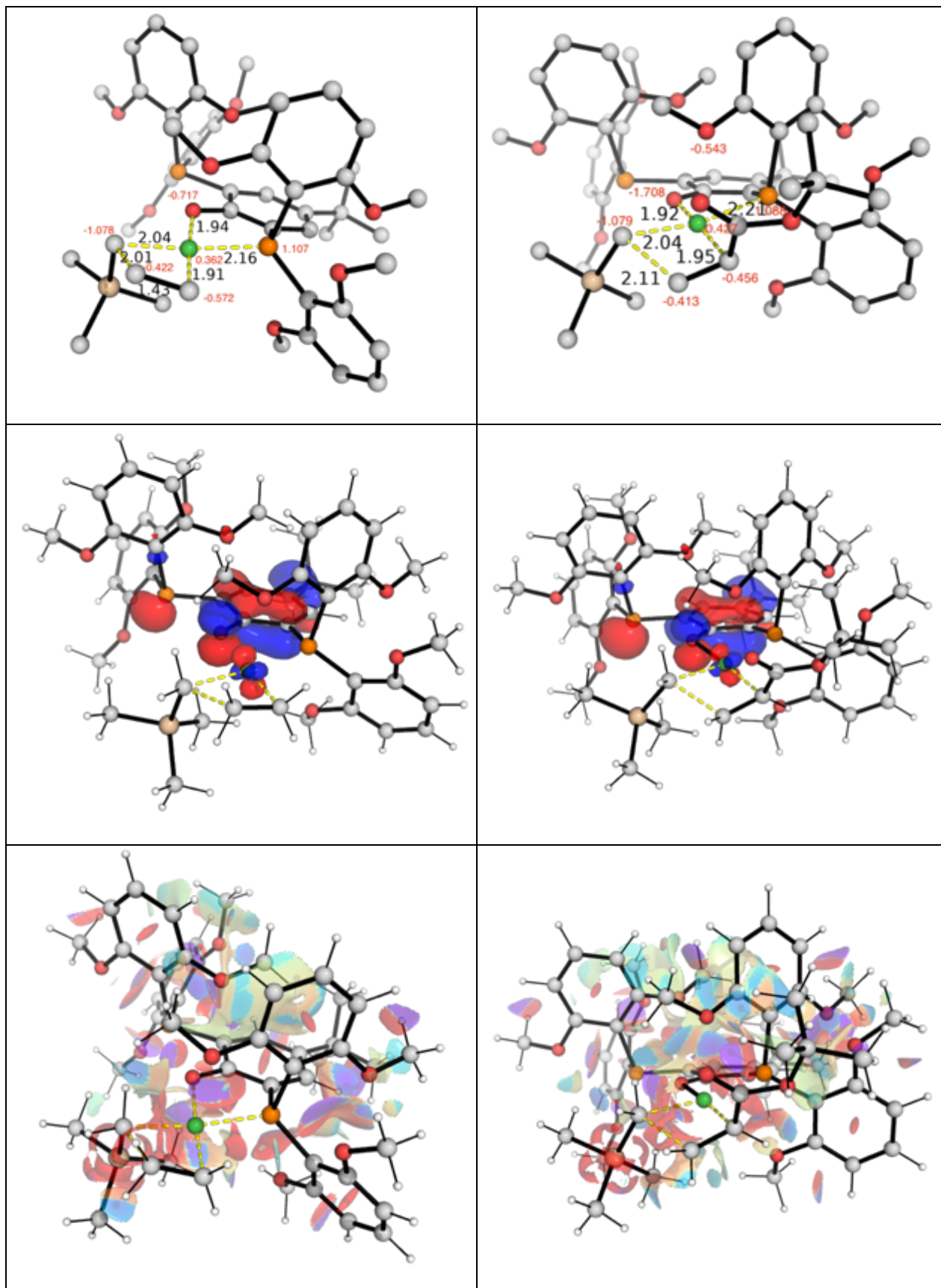


**Figure S9.13.** Optimized TS structures (first row), HOMO (middle row) and NCI plots (last row) for the isomerization of catalyst (**ts-5coord**), the isomerization of first ethylene-insertion product (**ts-5coord-et**) and the isomerization of first tBA-insertion product (**ts-5coord-ac**). Natural bond orbital (NBO) charges are given in red in the first row. Key bond distances are given in Å and angles are given in degrees. Isomerization barriers are given in kcal mol<sup>-1</sup>.

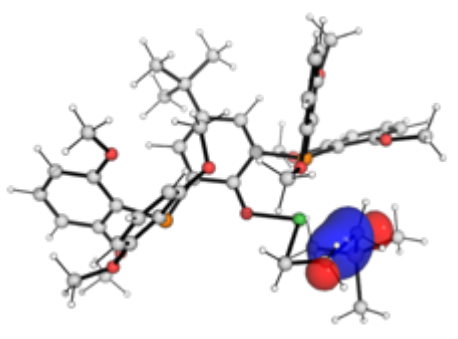
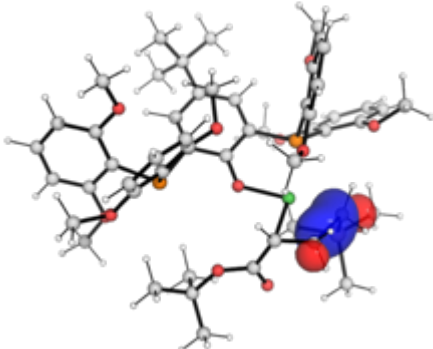
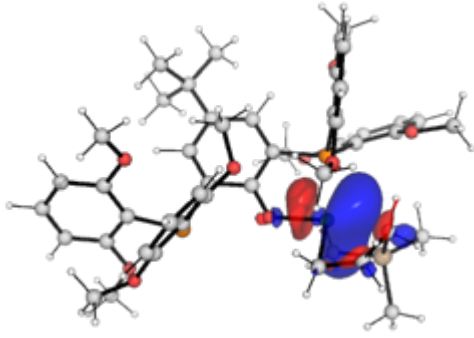
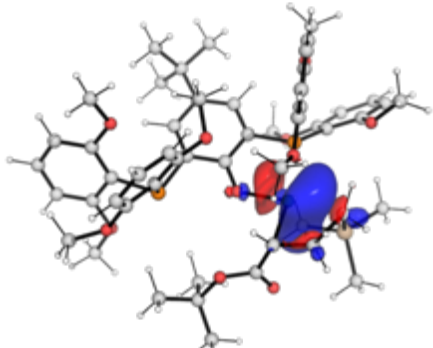
### 9.3.2 Comparison of sterics and electronics of first insertion

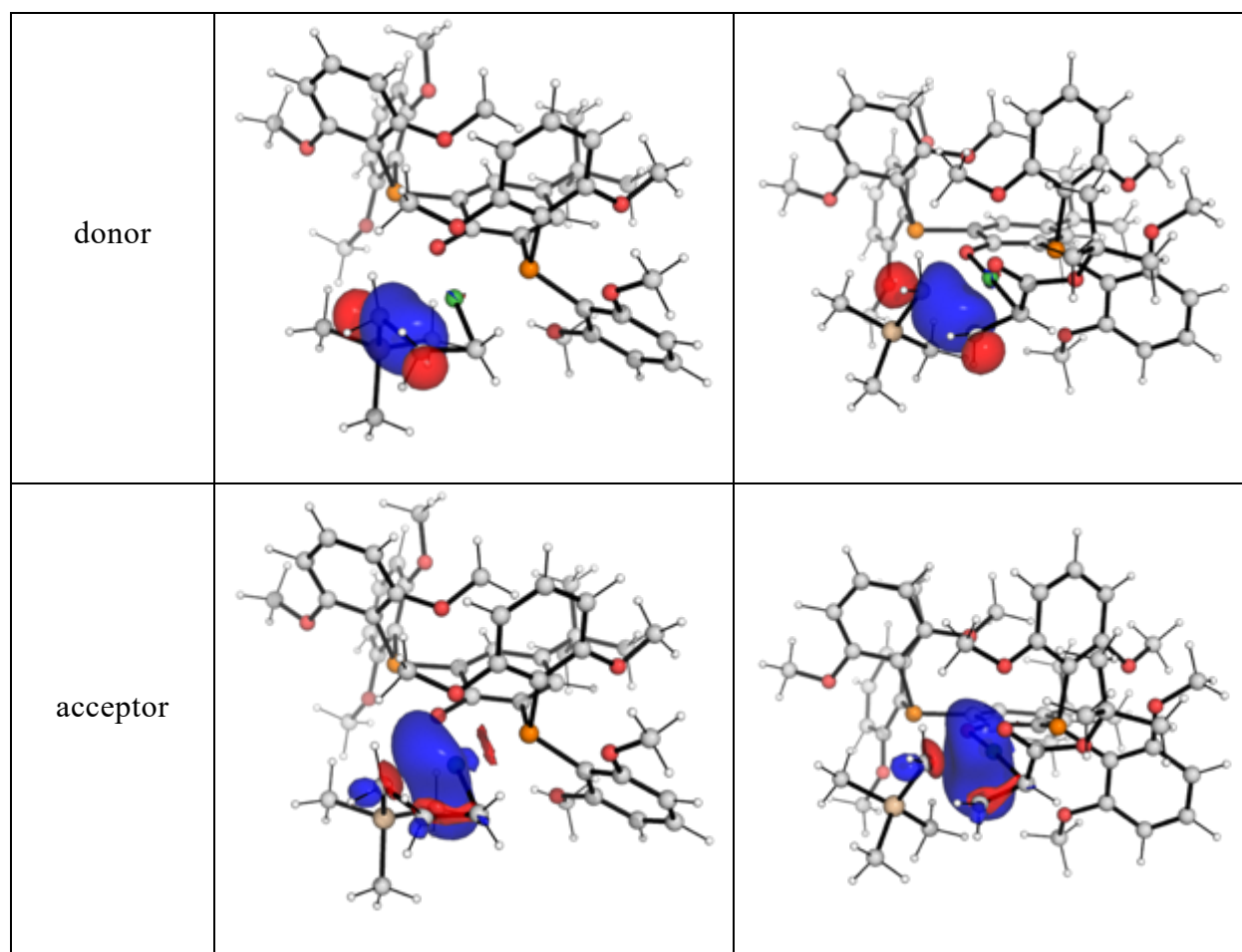






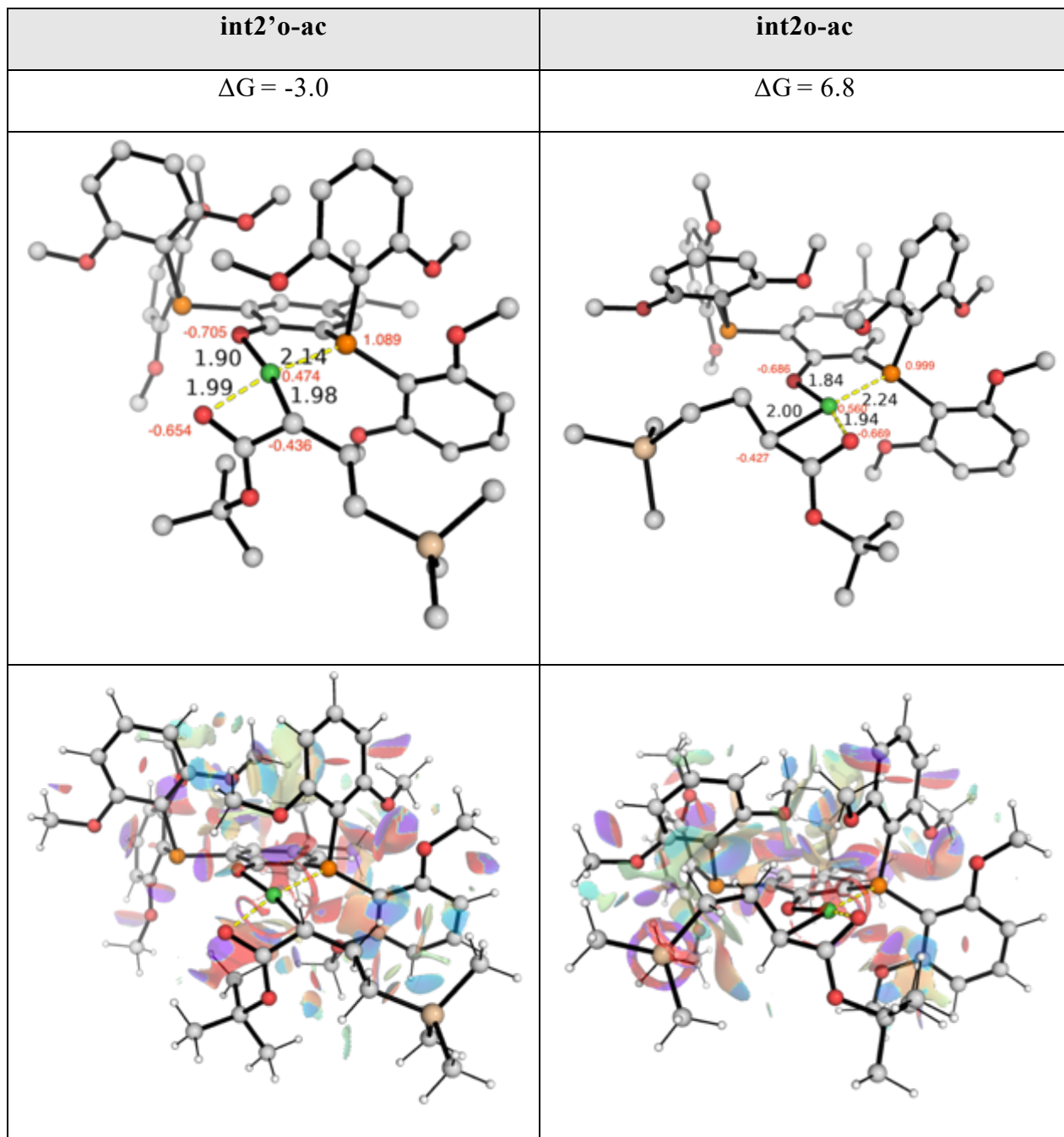
**Figure S9.14.** Optimized TS structures (first row), HOMO (middle row) and NCI plots (last row) for the first insertion into catalyst **1** and **1'**. Natural bond orbital (NBO) charges are given in red in the first row. TS free energies are relative to catalyst **1** and are given in kcal mol<sup>-1</sup>. Key bond distances are given in Å.

	<b>ts1-et</b>	<b>ts1-ac</b>
$\Delta E^{(2)}$	-58.8	-66.2
donor		
acceptor		
	<b>ts1'-et</b>	<b>ts1'-ac</b>
$\Delta E^{(2)}$	-76.8	-89.1

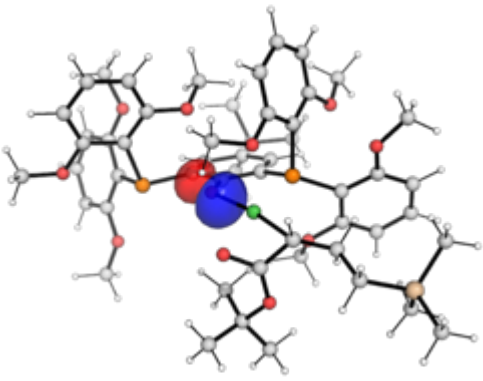
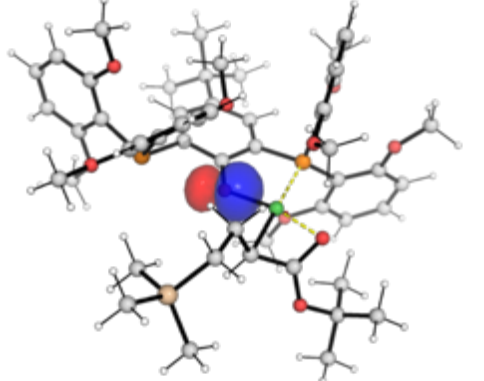
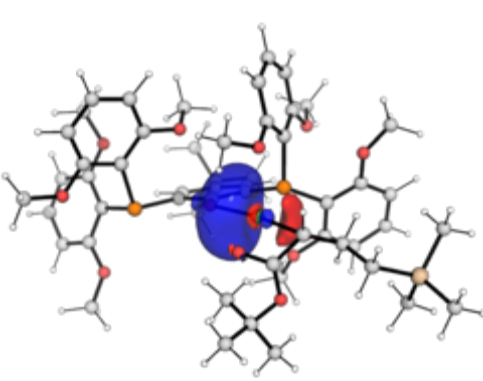
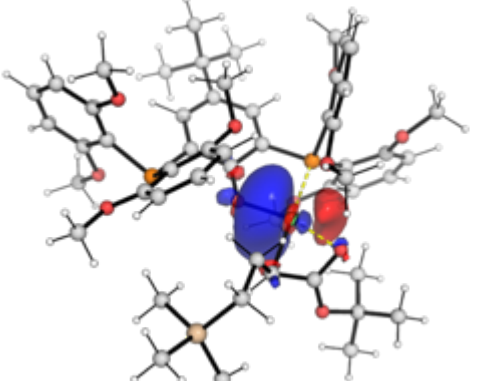


**Figure S9.15.** Natural bonding orbital (NBO) analysis using second-order perturbative stabilization energy ( $\Delta E^{(2)}$ ), which gives the dominant bonding interactions between the nascently formed C–C  $\sigma$ -bond and the metal (Ni  $d^*$  orbital). Energies are given in kcal mol<sup>-1</sup>.

### 9.3.3 Comparison of sterics and electronics of O-chelates



**Figure S9.16.** Optimized O-chelate structures from catalyst **1** and **1'** after first insertion of tBA monomer (first row) and their associated NCI plots (last row). Natural bond orbital (NBO) charges are given in red in the first row. Free energies are relative to catalyst **1** and are given in kcal mol<sup>-1</sup>. Key bond distances are given in Å.

	int2'o-ac	int2o-ac
$\Delta E^{(2)}$	-90.2	-90.7
donor		
acceptor		

**Figure S9.17.** Natural bonding orbital (NBO) analysis using second-order perturbative stabilization energy ( $\Delta E^{(2)}$ ), which gives the dominant bonding interactions between the ligand (O lone pair) and the metal (Ni  $d^*$  orbital). Energies are given in kcal mol<sup>-1</sup>.

#### 9.4 Optimized geometries

Geometries of all optimized structures (in .xyz format with their associated energy in Hartrees) are included in a separate folder named *ESI\_final\_structures\_xyz* with an associated README file. All these data have been deposited with this Supporting Information and uploaded to zenodo.org (DOI: 10.5281/zenodo.4593551).

## 9.5 Absolute energies, zero-point energies

Absolute values (in Hartrees) for SCF energy, zero-point vibrational energy (ZPE), enthalpy (H), entropy (T.S), Gibbs energy (G) and quasi-harmonic Gibbs energy (qh-G) (at 363K) for optimized structures are given below. Single point corrections in SMD chlorobenzene (PhCl) using M06/def2-TZVPP is also included.

Structure	E/au	ZPE/au	H/au	T.S/au	G/au	qh-G/au	SP M06 (PhCl)
pyridine	-247.909697	0.088228	-247.81546	0.032832	-247.848294	-247.848297	-248.1904562
acrylate	-423.819507	0.17752	-423.62895	0.04875	-423.677704	-423.676995	-424.3033801
ethylene	-78.455265	0.050271	-78.400563	0.02478	-78.425344	-78.425344	-78.54851714
<b>1</b>	-5189.241603	1.036085	-5188.1233	0.198768	-5188.3221	-5188.305872	-5192.797515
<b>1-c2</b>	-5189.236897	1.036548	-5188.1183	0.197557	-5188.31588	-5188.3003	-5192.782739
<b>1a</b>	-5189.212702	1.034707	-5188.0954	0.199746	-5188.29511	-5188.279103	-5192.765101
<b>1b</b>	-5189.185522	1.034698	-5188.0679	0.205235	-5188.27313	-5188.253497	-5192.75056
<b>1c</b>	-5189.186621	1.035603	-5188.0688	0.200136	-5188.26894	-5188.25173	-5192.748144
<b>1d</b>	-5189.194589	1.034687	-5188.0778	0.196656	-5188.27445	-5188.259757	-5192.744988
<b>1e</b>	-5189.196931	1.034702	-5188.0798	0.200321	-5188.28009	-5188.263164	-5192.75054
<b>1'</b>	-5189.231303	1.036112	-5188.1132	0.197377	-5188.31058	-5188.295063	-5192.791076
<b>1'-c2</b>	-5189.23134	1.03661	-5188.113	0.196555	-5188.30957	-5188.29421	-5192.791052
<b>1-et</b>	-5267.706362	1.088281	-5266.5311	0.209256	-5266.7404	-5266.723044	-5271.353245
<b>1'-et</b>	-5267.694985	1.091389	-5266.5188	0.201332	-5266.72017	-5266.705166	-5271.333264
<b>1-5coord</b>	-5189.242184	1.037125	-5188.1233	0.196911	-5188.32024	-5188.304669	-5192.796841
<b>ts-5coord</b>	-5189.199468	1.035075	-5188.0832	0.194773	-5188.27798	-5188.263332	-5192.754707



<b>ts-5coord-c2</b>	-5189.201204	1.036326	-5188.0839	0.195138	-5188.27908	-5188.26383	-5192.75408
<b>ts-tet</b>	-5189.18503	1.033482	-5188.069	0.201988	-5188.27094	-5188.253244	-5192.744506
<b>ts-tet-c2</b>	-5189.184899	1.034553	-5188.0682	0.200527	-5188.26873	-5188.251449	-5192.744486
<b>1-3coord</b>	-4941.274167	0.944664	-4940.2542	0.184598	-4940.43882	-4940.423931	-4944.560212
<b>ts-3coord</b>	-4941.235107	0.943599	-4940.2156	0.18711	-4940.40269	-4940.387171	-4944.526758
<b>1'-3coord</b>	-4941.267226	0.945768	-4940.2459	0.184686	-4940.43058	-4940.416053	-4944.555098
<b>int1-et-c1</b>	-5019.769048	0.999264	-5018.6903	0.192846	-5018.88313	-5018.867915	-5023.13828
<b>int1-et-c2</b>	-5019.755394	0.999292	-5018.6765	0.193086	-5018.86955	-5018.854351	-5023.128822
<b>ts1-et</b>	-5019.732137	0.99937	-5018.6543	0.190634	-5018.84495	-5018.829914	-5023.100743
<b>int2-et-5m</b>	-5019.759654	1.001171	-5018.6801	0.189694	-5018.86977	-5018.855275	-5023.127892
<b>int2-et</b>	<b>-5019.774032</b>	<b>1.000902</b>	<b>-5018.6949</b>	<b>0.190244</b>	<b>-5018.88517</b>	<b>-5018.870031</b>	<b>-5023.143109</b>
<b>int2-et-py</b>	-5267.720861	1.091861	-5266.5437	0.205831	-5266.74954	-5266.732392	-5271.363807
<b>int3-et-et</b>	-5098.259105	1.056309	-5097.121	0.196427	-5097.31747	-5097.302357	-5101.713874
<b>ts3-et-et</b>	-5098.254169	1.056623	-5097.1167	0.193558	-5097.31023	-5097.296119	-5101.707965
<b>int4-et-et-5m</b>	-5098.286035	1.059077	-5097.1461	0.193002	-5097.33914	-5097.325121	-5101.736877
<b>int4-et-et</b>	-5098.278376	1.057475	-5097.1391	0.201245	-5097.34036	-5097.322692	-5101.740405
<b>int4-et-et-py</b>	-5346.233736	1.147978	-5344.9972	0.215569	-5345.2128	-5345.193162	-5349.963406
<b>int3-et-ac-o1</b>	-5443.613849	1.181021	-5442.3407	0.218123	-5442.55883	-5442.541496	-5447.455874
<b>ts3-et-ac-c2</b>	-5443.629067	1.18354	-5442.3555	0.211645	-5442.56719	-5442.551629	-5447.467354
<b>int3-et-ac</b>	-5443.634197	1.184165	-5442.3597	0.211941	-5442.57163	-5442.556291	-5447.471049

<b>ts3-et-ac</b>	-5443.632409	1.183665	-5442.3589	0.211135	-5442.57005	-5442.554611	-5447.469085
<b>int4-et-ac-5m</b>	-5443.666668	1.185743	-5442.3908	0.211901	-5442.60274	-5442.58715	-5447.502749
<b>int4-et-ac</b>	-5443.663361	1.182787	-5442.3889	0.2225	-5442.61135	-5442.591162	-5447.507477
<b>int4o-et-ac</b>	-5443.667926	1.182892	-5442.3932	0.222185	-5442.61534	-5442.595293	-5447.509146
<b>int4-et-ac-py</b>	-5691.613601	1.275918	-5690.2402	0.234284	-5690.47448	-5690.452908	-5695.726293
<b>int1-ac-o1</b>	-5365.14382	1.126406	-5363.929	0.20859	-5364.13755	-5364.122284	-5368.896838
<b>int1-ac-o2</b>	-5365.139406	1.126901	-5363.9242	0.209643	-5364.13388	-5364.117481	-5368.895341
<b>int1-ac-c2</b>	-5365.14134	1.127254	-5363.9264	0.206149	-5364.13255	-5364.117725	-5368.892272
<b>int1-ac-c1</b>	-5365.137787	1.126468	-5363.9227	0.211357	-5364.13409	-5364.116908	-5368.892686
<b>int1-ac-c4</b>	-5365.124659	1.127448	-5363.9095	0.206261	-5364.11579	-5364.101063	-5368.877123
<b>ts1-ac-r</b>	-5365.095363	1.125928	-5363.8818	0.209193	-5364.09102	-5364.074341	-5368.848503
<b>int2-ac-r-5m</b>	-5365.122976	1.126293	-5363.9083	0.212228	-5364.12057	-5364.102883	-5368.876551
<b>int2-ac-r</b>	-5365.140289	1.129117	-5363.9245	0.205681	-5364.13022	-5364.114439	-5368.898534
<b>int2o-ac-r</b>	-5365.151173	1.128006	-5363.9356	0.208853	-5364.14442	-5364.127689	-5368.905791
<b>int1-ac-c3</b>	-5365.132432	1.12721	-5363.9174	0.20718	-5364.12455	-5364.109338	-5368.884794
<b>ts1-ac</b>	-5365.117188	1.126246	-5363.9033	0.20831	-5364.11158	-5364.095714	-5368.866499
<b>int2-ac-5m</b>	-5365.145081	1.129101	-5363.9289	0.206478	-5364.1354	-5364.119609	-5368.892552
<b>int2-ac</b>	-5365.150976	1.128597	-5363.935	0.20689	-5364.14186	-5364.126473	-5368.903844
<b>int2o-ac</b>	-5365.152768	1.128034	-5363.9367	0.209688	-5364.14642	-5364.129761	-5368.905835
<b>int2-ac-py</b>	-5613.11037	1.218904	-5611.7974	0.222257	-5612.01966	-5612.001677	-5617.134478

<b>int3-ac-et</b>	-5443.631637	1.183465	-5442.3573	0.214522	-5442.5718	-5442.555477	-5447.473936
<b>ts3-ac-et</b>	-5443.619682	1.183437	-5442.3462	0.212359	-5442.55852	-5442.542498	-5447.461815
<b>ts3-ac-et-c2</b>	-5443.6109	1.184377	-5442.3369	0.209489	-5442.54643	-5442.531757	-5447.448411
<b>int4-ac-et- 5m</b>	-5443.663307	1.184668	-5442.3881	0.213211	-5442.60126	-5442.585479	-5447.500983
<b>int4-ac-et</b>	-5443.645335	1.181883	-5442.3726	0.22009	-5442.59264	-5442.572673	-5447.492232
<b>int4o-ac-et</b>	-5443.674743	1.186755	-5442.3989	0.207929	-5442.60685	-5442.592145	-5447.512689
<b>int4-ac-et- py</b>	-5691.603271	1.274271	-5690.2308	0.238781	-5690.46956	-5690.445934	-5695.723481
<b>int3-ac-ac</b>	-5789.00125	1.308686	-5787.5919	0.234642	-5787.82652	-5787.808407	-5793.22464
<b>ts3-ac-ac</b>	-5788.997784	1.309946	-5787.5885	0.229713	-5787.81824	-5787.801633	-5793.221201
<b>ts3-ac-ac-c2</b>	-5788.99554	1.309709	-5787.5861	0.232168	-5787.81826	-5787.800354	-5793.220172
<b>ts3-ac-ac-c3</b>	-5788.983713	1.310518	-5787.5739	0.23197	-5787.80589	-5787.787367	-5793.206716
<b>int4-ac-ac- 5m</b>	-5789.029337	1.311337	-5787.618	0.232981	-5787.85102	-5787.832913	-5793.256034
<b>int4-ac-ac</b>	-5789.037769	1.311353	-5787.6271	0.231676	-5787.85875	-5787.840622	-5793.262425
<b>int4o-ac-ac</b>	-5789.057057	1.313791	-5787.645	0.226446	-5787.87144	-5787.855275	-5793.275367
<b>int4-ac-ac- py</b>	-6036.986375	1.401863	-6035.4776	0.251979	-6035.72956	-6035.706971	-6041.486186
<b>int1'-ac-o1</b>	-5365.123621	1.125321	-5363.9096	0.211759	-5364.12132	-5364.103989	-5368.880059
<b>int1'-ac-o2</b>	-5365.119695	1.125119	-5363.9058	0.210161	-5364.11599	-5364.099864	-5368.876718
<b>int1'-ac-c1</b>	-5365.136514	1.125243	-5363.9225	0.210529	-5364.13305	-5364.116795	-5368.889853
<b>int1'-ac-c2</b>	-5365.135934	1.127289	-5363.9208	0.206553	-5364.12738	-5364.112707	-5368.887566

<b>int1'-ac-c3</b>	-5365.129584	1.126723	-5363.9147	0.211079	-5364.12577	-5364.108177	-5368.884062
<b>ts1'-ac-r</b>	-5365.118221	1.12636	-5363.9044	0.208669	-5364.11311	-5364.096233	-5368.871442
<b>int2'-ac-r-</b>							
<b>5m</b>	-5365.141155	1.128051	-5363.9255	0.209702	-5364.13519	-5364.117982	-5368.894135
<b>int2'-ac-r</b>	-5365.142024	1.129869	-5363.9253	0.20607	-5364.13142	-5364.115458	-5368.89758
<b>int2'o-ac-r</b>	-5365.161022	1.128933	-5363.9447	0.20854	-5364.15325	-5364.136533	-5368.919239
<b>int1'-ac-c4</b>	-5365.132373	1.127515	-5363.9171	0.207739	-5364.12482	-5364.109235	-5368.88387
<b>ts1'-ac</b>	-5365.128369	1.127405	-5363.9139	0.205761	-5364.11964	-5364.10461	-5368.879545
<b>ts1'-ac-c2</b>	-5365.13104	1.128037	-5363.9163	0.20397	-5364.12024	-5364.105858	-5368.880289
<b>int2'-ac-5m</b>	-5365.159411	1.128809	-5363.943	0.207833	-5364.15084	-5364.135078	-5368.91004
<b>int2'-ac</b>	-5365.159959	1.128007	-5363.9443	0.208652	-5364.15294	-5364.136532	-5368.912959
<b>int2'o-ac</b>	-5365.167805	1.127878	-5363.9518	0.211468	-5364.16327	-5364.145649	-5368.920537
<b>int2'-ac-py</b>	-5613.113548	1.218963	-5611.8	0.225777	-5612.0258	-5612.006061	-5617.140639
<b>ts-5coord-ac</b>	-5613.072434	1.216883	-5611.7611	0.226015	-5611.98715	-5611.967451	-5617.096872
<b>int3'-ac-et</b>	-5443.626601	1.182244	-5442.3525	0.218262	-5442.57076	-5442.552981	-5447.468885
<b>ts3'-ac-et</b>	-5443.598075	1.181525	-5442.3256	0.216397	-5442.54195	-5442.524543	-5447.4407
<b>int4'-ac-et-</b>							
<b>5m</b>	-5443.629021	1.183632	-5442.3544	0.216486	-5442.57087	-5442.553354	-5447.470218
<b>int4'-ac-et</b>	-5443.634584	1.18283	-5442.3603	0.221897	-5442.5822	-5442.561955	-5447.481968
<b>int4'o-ac-et</b>	-5443.64984	1.183962	-5442.3749	0.219313	-5442.5942	-5442.574868	-5447.493738
<b>int4'-ac-et-</b>							
<b>py</b>	-5691.588782	1.275829	-5690.2158	0.232709	-5690.44847	-5690.427263	-5695.707557

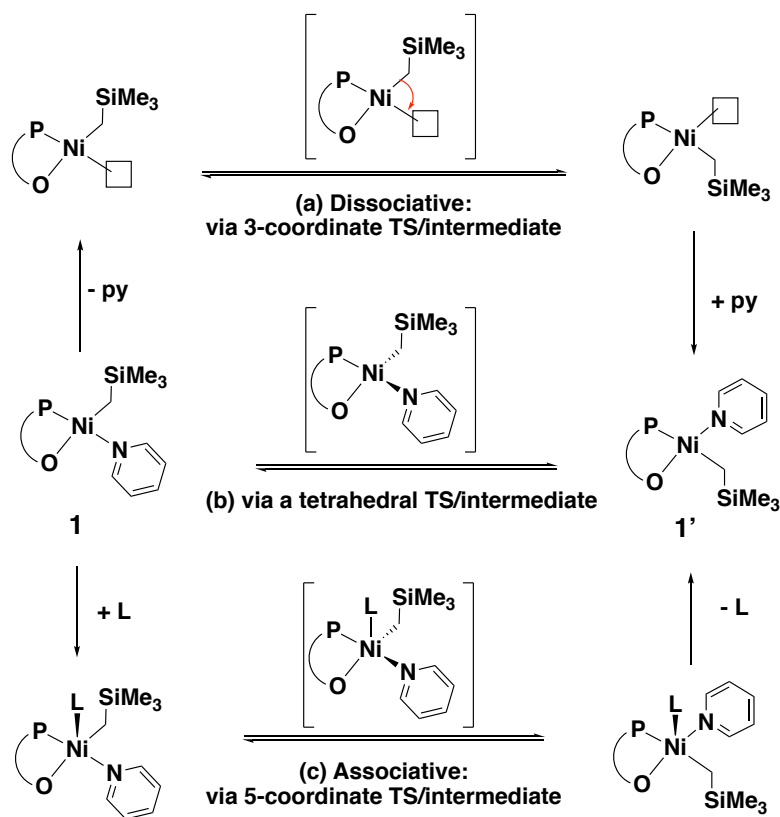
<b>int3'-ac-ac</b>	-5789.004047	1.310423	-5787.5935	0.232865	-5787.82635	-5787.808218	-5793.226696
<b>ts3'-ac-ac</b>	-5788.981456	1.309115	-5787.5723	0.234356	-5787.80663	-5787.78763	-5793.205127
<b>int4'-ac-ac-</b>							
<b>5m</b>	-5789.012895	1.310839	-5787.6026	0.232658	-5787.83529	-5787.816658	-5793.234135
<b>int4'-ac-ac</b>	-5789.017714	1.310426	-5787.6071	0.236439	-5787.84356	-5787.823463	-5793.243263
<b>int4'o-ac-ac</b>	-5789.034041	1.311631	-5787.6225	0.235154	-5787.8577	-5787.838042	-5793.253317
<b>int4'-ac-ac-</b>							
<b>py</b>	-6036.974438	1.402495	-6035.4657	0.249163	-6035.71486	-6035.693067	-6041.474135
<b>int1'-et-c1</b>	-5019.76831	0.998667	-5018.6903	0.191812	-5018.88207	-5018.86728	-5023.133637
<b>int1'-et-c2</b>	-5019.761944	0.999589	-5018.6833	0.191266	-5018.87456	-5018.859808	-5023.130173
<b>ts1'-et</b>	-5019.752934	0.998849	-5018.6755	0.191288	-5018.86675	-5018.851419	-5023.120112
<b>int2'-et-5m</b>	-5019.776492	1.000064	-5018.6974	0.1929	-5018.89025	-5018.874367	-5023.143195
<b>int2'-et</b>	-5019.783341	1.000021	-5018.7043	0.193669	-5018.89794	-5018.881715	-5023.151533
<b>int2'-et-c1</b>	-5019.780706	1.000697	-5018.7014	0.191526	-5018.89294	-5018.877463	-5023.152537
<b>int2'-et-c2</b>	-5019.780994	1.000541	-5018.7018	0.19144	-5018.89321	-5018.877944	-5023.148888
<b>int2'-et-py</b>	-5267.730378	1.092304	-5266.553	0.206432	-5266.75943	-5266.741747	-5271.372532
<b>ts-5coord-et</b>	-5267.699152	1.091151	-5266.5236	0.204065	-5266.72767	-5266.7107	-5271.342345
<b>int3'-et-et</b>	-5098.268091	1.055728	-5097.1302	0.197407	-5097.32765	-5097.31252	-5101.722032
<b>ts3'-et-et</b>	-5098.232948	1.056302	-5097.0954	0.196573	-5097.29193	-5097.276314	-5101.690656
<b>int4'-et-et-</b>							
<b>5m</b>	-5098.263033	1.056901	-5097.1243	0.197586	-5097.32192	-5097.306427	-5101.71945
<b>int4'-et-et</b>	-5098.268635	1.055862	-5097.1305	0.204279	-5097.33474	-5097.315819	-5101.731631

<b>int4'-et-et- py</b>	-5346.223791	1.149681	-5344.9866	0.209814	-5345.19644	-5345.179198	-5349.957613
<b>int3'-et-ac</b>	-5443.630788	1.183882	-5442.3561	0.2133	-5442.56941	-5442.553492	-5447.470966
<b>ts3'-et-ac</b>	-5443.617916	1.183706	-5442.344	0.213136	-5442.55709	-5442.540818	-5447.456116
<b>int4'-et-ac- 5m</b>	-5443.647073	1.184454	-5442.372	0.214202	-5442.58616	-5442.569823	-5447.484278
<b>int4'-et-ac</b>	-5443.650879	1.184302	-5442.3758	0.217637	-5442.59342	-5442.575112	-5447.494123
<b>int4'o-et-ac</b>	-5443.654172	1.184072	-5442.3789	0.217757	-5442.59663	-5442.578655	-5447.497208
<b>int4'-et-ac- py</b>	-5691.610865	1.275926	-5690.2379	0.229741	-5690.46767	-5690.448546	-5695.719416

---

## 10. Computational investigation in isomerization

The isomerization of the square planar catalyst between **POP-Ni-py (1)** and its isomeric form **POP-Ni-py 1'** can occur via one of the three possible mechanisms: associative, dissociative or twisting through a tetrahedral TS and then back to square planar. This step is essential for the insertion of ethylene into the Ni–C bond via the lower TS **ts1'-et**, at 20.5 kcal mol<sup>-1</sup>, rather than via **ts1-et**, at 33.1 kcal mol<sup>-1</sup>. We herein consider these possibilities computationally:



**Scheme S10.1.** Possible mechanisms of isomerization between two geometric isomeric forms of the Ni-catalyst.

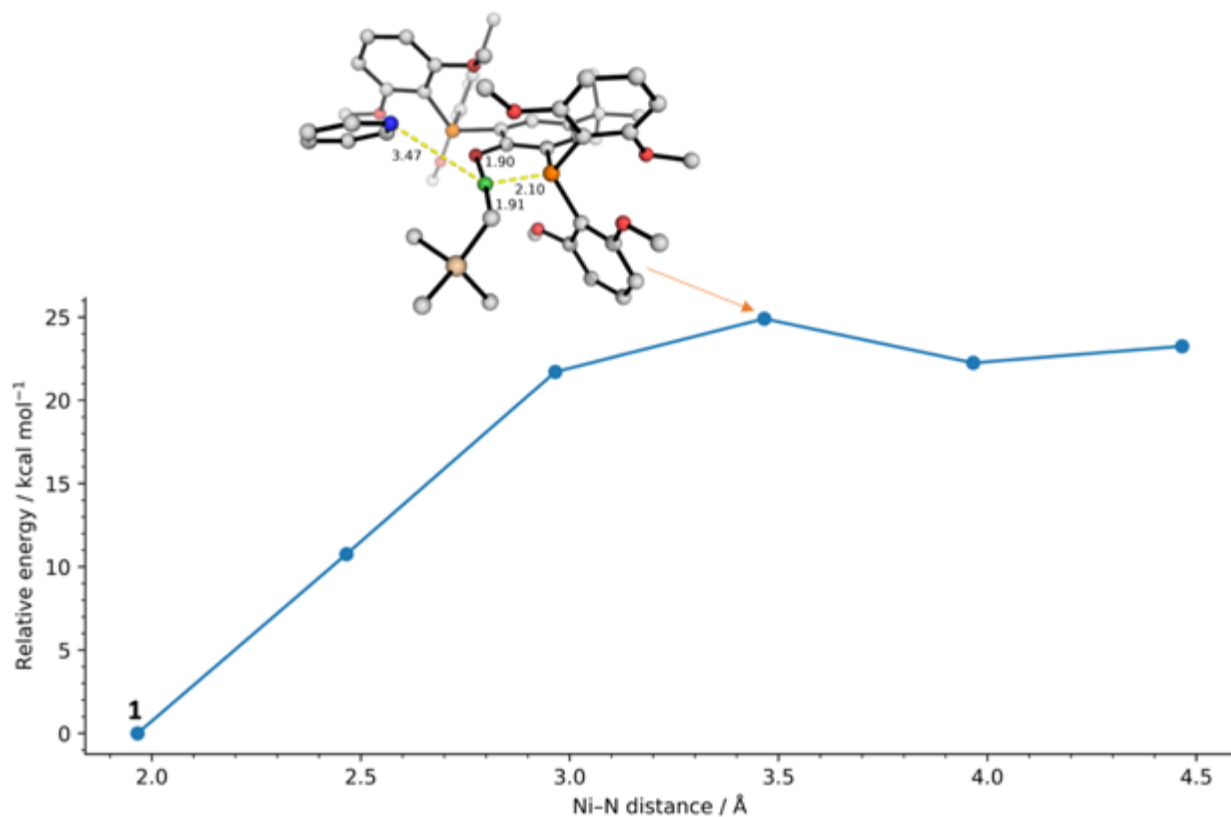
### 10.1 Dissociative mechanism

In a dissociative mechanism, the coordinating pyridine ligand leaves, giving a vacant site on Ni metal. Subsequently, the growing polymer chain can isomerize by moving from its original coordinating site to its adjacent, newly vacated coordination site. This is followed by

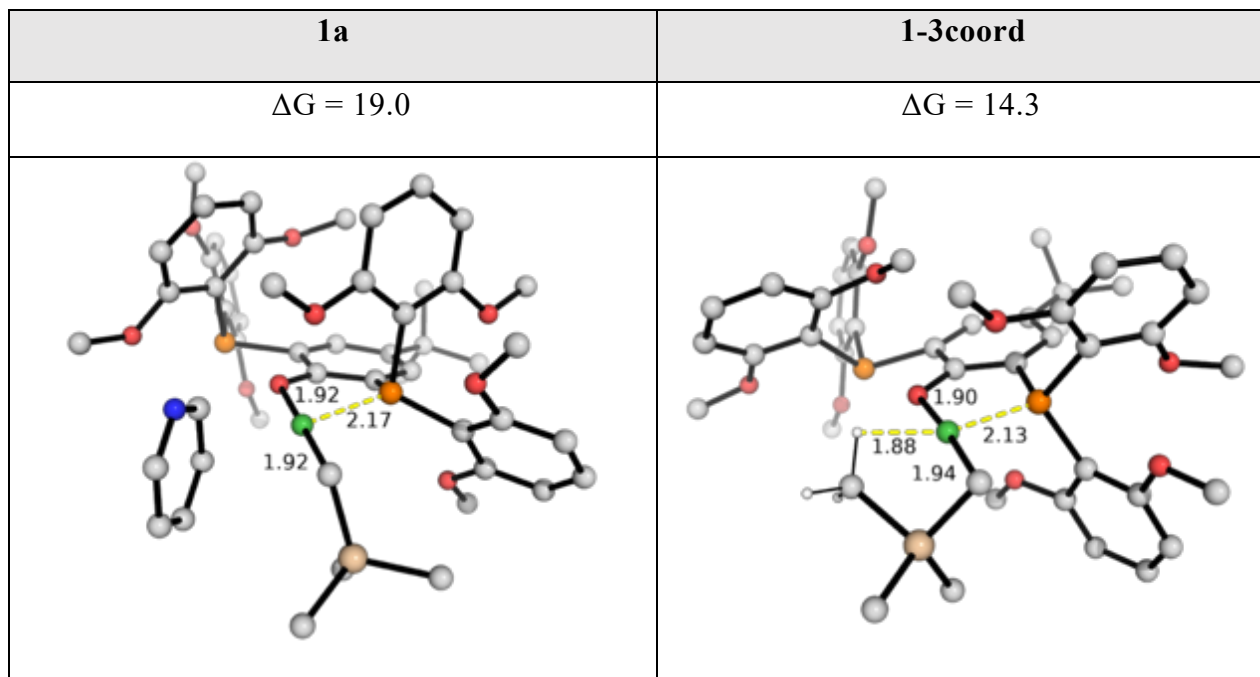
recoordination of pyridine ligand at the site previously occupied by the growing polymer chain, giving the geometric isomeric form of the catalyst (Scheme S10.1a).

We first try to estimate the barrier to pyridine dissociation by doing a relaxed PES scan along the Ni–N(pyridine) bond. The gas phase energy scan is given in Figure S10.1. We can see that the loss of pyridine ligand is unfavorable and reversible. This is consistent with geometry optimization starting from initial guess structure of long (3.70 Å) Ni–N(pyridine) bond (by manually increasing this distance in catalyst **1** while maintaining the square plane of the Ni-center) which optimized back to catalyst **1**. To obtain the accurate Gibbs energy with solvent correction for the resulting structure after loss of pyridine coordination, we took the structure at point 5 in Figure S10.1 and subjected it to geometry optimization. The final structure, **1a**, is 19.0 kcal mol<sup>-1</sup> uphill (Figure S10.2). This gives the estimate of the dissociation barrier of pyridine as *ca.* 22 kcal mol<sup>-1</sup> (this is nonetheless smaller than the isomerization barrier, *vide infra*). The loss of pyridine from this species, displaced by an agnostic interaction from the C–H group on trimethylsilyl, gives **1-3coord** which is 14.3 kcal mol<sup>-1</sup> uphill (Figure S10.2). This species can further undergo isomerization to give the species **1-3coord** at 18.1 kcal mol<sup>-1</sup> relative to catalyst **Ni-POP-py 1**.





**Figure S10.1.** Relaxed PES scan along phenoxide O-Ni-C angle going from one 3-coordinate isomer to another. Relative energy values are computed at M06/def2-SVP in gas phase and used without further corrections. Key bond distances are given in Å.



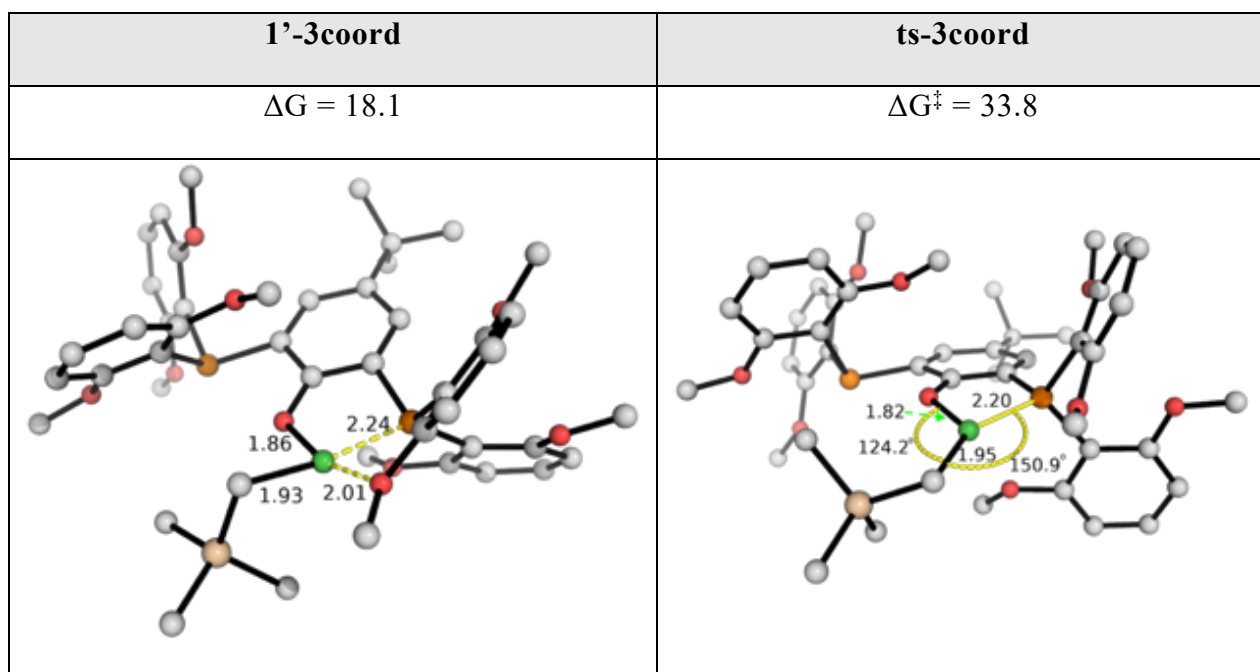


**Figure S10.2.** Optimized structures for the coordination complexes of the isomeric Ni-catalyst **1** and **1'** after losing pyridine coordination to give 3-coordinate species and the TS structure for the isomerization via 3-coordinate TS. The Gibbs energies are calculated relative to **POP-Ni-py (1)**. Key bond distances are given in Å and angles are given in degrees. Gibbs energy units are given in kcal mol<sup>-1</sup>.

Therefore, the loss of pyridine from catalyst **1** gives **1-3coord**, at 14.3 kcal mol<sup>-1</sup>. We next set out to find the TS for the isomerization from **1-3coord** to **1'-3coord**. We initially tried direct TS search using the guess structure of placing the polymer chain in between the two Ni-coordination sites and QST2 method (in Gaussian 16 software, both *opt=modredundant* and *opt=qst2* methods) to no avail. We can, however, do a relaxed PES scan sweeping out the angle from one geometric isomer to the other to get an estimate of the barrier for such isomerization. This relaxed PES scan in gas phase is given in Figure S10.3, allowing us to estimate that the barrier for the isomerization from **1-3coord** to **1'-3coord** is about 24 kcal mol<sup>-1</sup>. This estimate is valid since the energy difference between **1-3coord** and **1'-3coord** in the gas phase ( $\Delta\Delta E = 4.4$  kcal mol<sup>-1</sup>) is very similar to their Gibbs energy difference in solvent ( $\Delta\Delta G = 3.8$  kcal mol<sup>-1</sup>). Given that species **1-3coord** is 14.3 kcal mol<sup>-1</sup> uphill with respect to **Ni-POP-py 1**, we estimate that the barrier for isomerization of catalyst **Ni-POP-py 1** to its geometric isomer **Ni-POP-py 1'** via a 3-coordinate TS has an upper bound activation barrier

of 38 kcal mol<sup>-1</sup>, which is much higher than the barriers for the migratory insertion of monomer into Ni–C bond of catalyst **Ni-POP-py 1** (Figure S9.4).

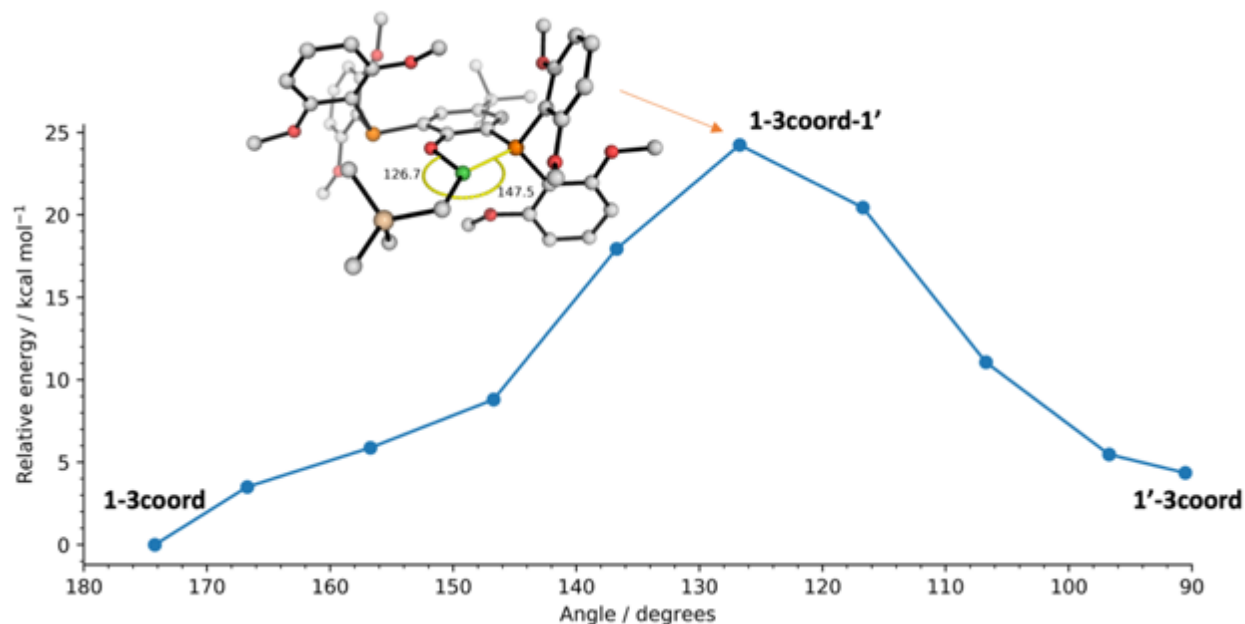


**Figure S10.3.** Relaxed PES scan along phenoxide O–Ni–C angle going from one 3-coordinate isomer to another. Relative energy values are computed at M06/def2-SVP in gas phase and used without further corrections. Key bond distances are given in Å.

Next, we took the structure with the highest energy from this PES scan (Figure S10.3) as an initial guess for the 3-coordinate isomerization TS search. We are able to locate the true TS **ts-3coord** (Figure S10.4, verified by IRC) having a barrier of 33.8 kcal mol<sup>-1</sup> relative to the catalyst **Ni-POP-py 1**.

In **1'-3coord** we see that the oxygen atom of an adjacent methoxy group on the ligand can coordinate to the Ni-metal. We wonder if this coordination can displace pyridine ligand in catalyst **1**, thus giving the isomeric **1'**. The optimized structures and their associated energetics are shown in Figure S10.4. The displacement of pyridine ligand by OMe group gives structure **1b**, which is endergonically uphill, at 27.1 kcal mol<sup>-1</sup>. This requires an activation barrier of at least 27.1 kcal mol<sup>-1</sup> and is unfavorable. This is perhaps unsurprising as a strong Ni–N(pyridine) interaction is lost and replaced by a weaker Ni–O(methoxy) interaction.

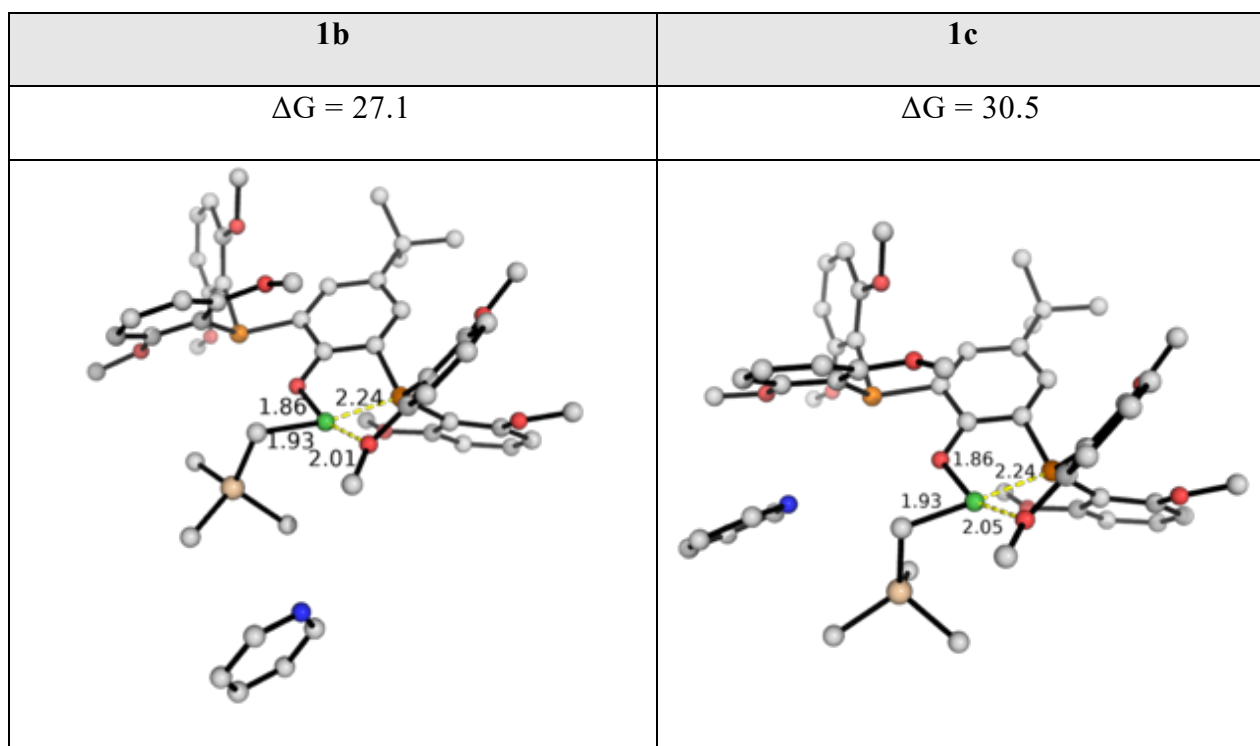
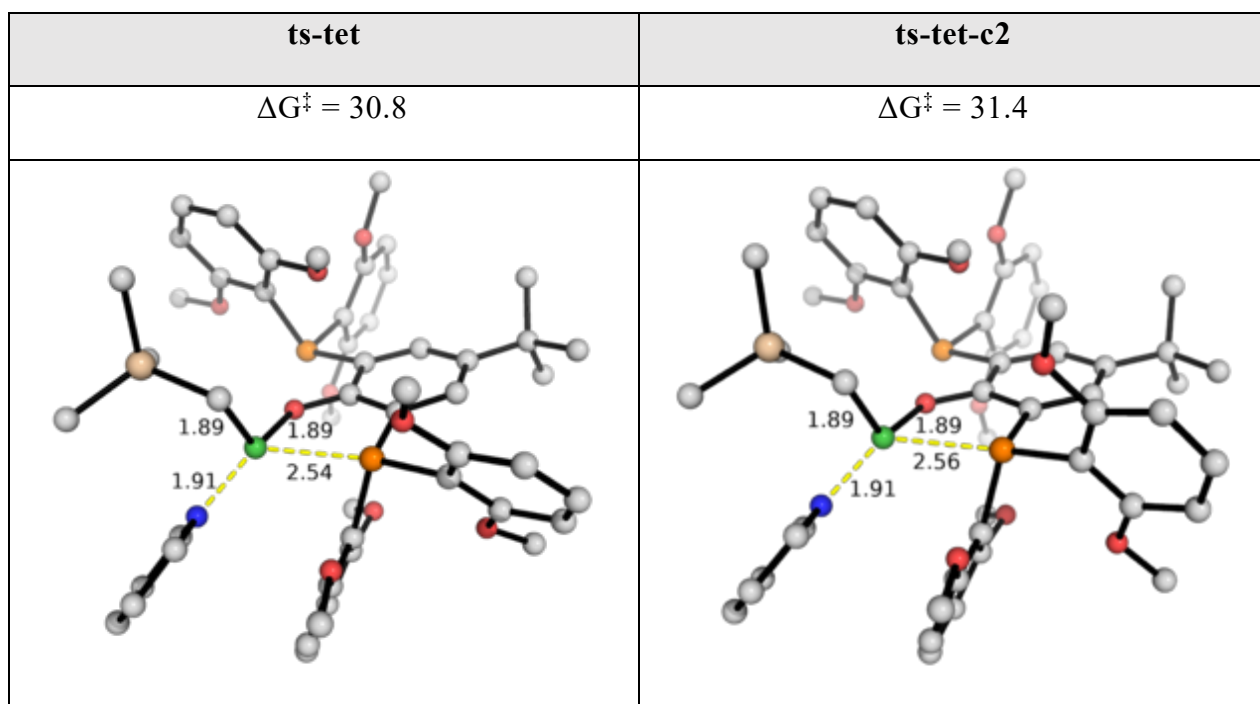


**Figure S10.4.** Optimized structures for the coordination complexes of the isomeric Ni-catalyst **1** and **1'** after losing pyridine coordination to give 3-coordinate species. The Gibbs energies are calculated relative to **POP-Ni-py (1)**. Key bond distances are given in Å. Gibbs energy units are given in kcal mol<sup>-1</sup>.

This dissociative mechanism has an overall barrier of 33.8 kcal mol<sup>-1</sup> which is higher than the isomerization barriers for the other two mechanistic possibilities (*vide infra*) and is thus unlikely for the isomerization of catalyst **1** to its geometric isomer **1'**.

## 10.2 Twisting mechanism via tetrahedral TS/intermediate

A similar dihedral angle scan mapping out one geometric isomer to the other passing through the tetrahedral TS/intermediate, to estimate how big the barrier is, was not successful due to the difficulties in defining the scanning coordinates. However, the direct TS search for the putative TS structure gives two TS conformers, **ts-tet** and **ts-tet-c2**, with the lowest activation barrier of 30.8 kcal mol<sup>-1</sup> (**ts-tet**, Figure S10.5). This TS has been verified to be the true TS for the isomerization via tetrahedral TS using IRC analyses.

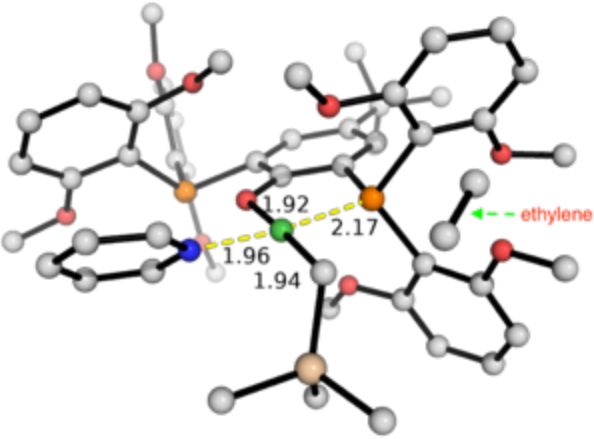
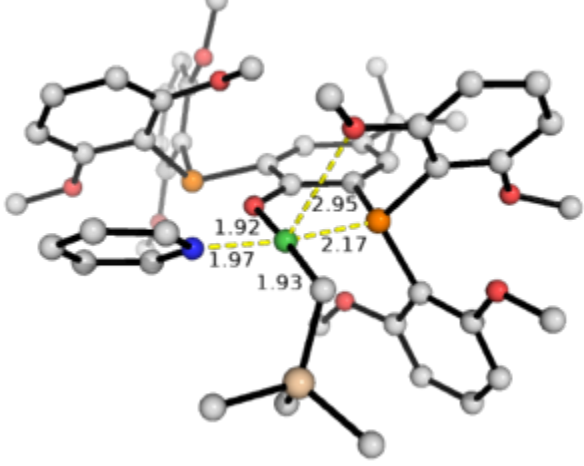
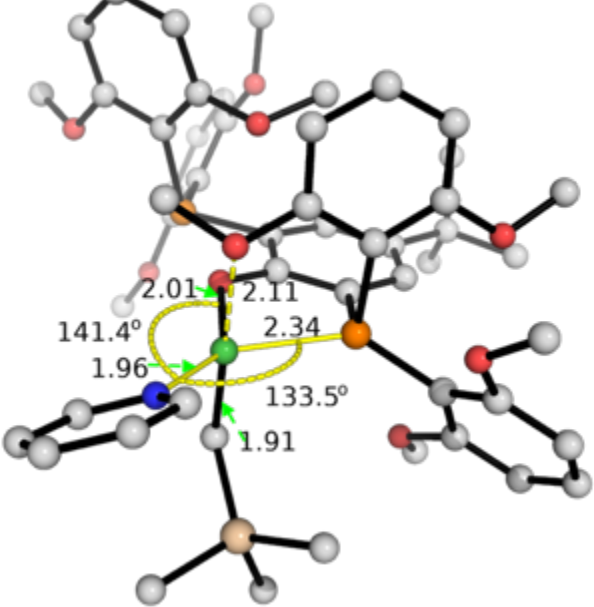
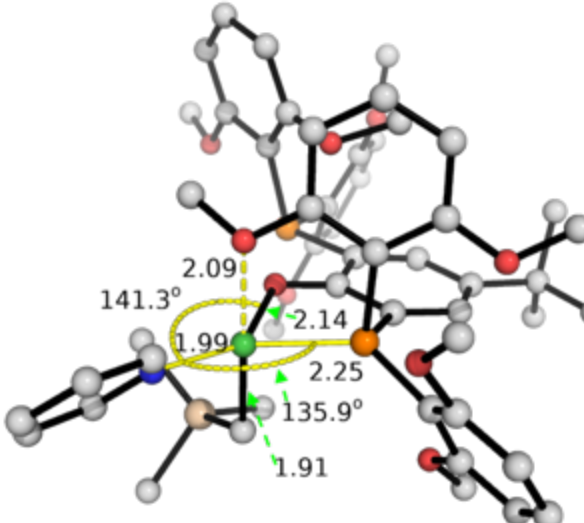


**Figure S10.5.** Optimized TS structures for the isomerization of catalyst **1** to **1'** via tetrahedral transition state. Two TS conformers were found. Key bond distances are given in Å. Gibbs energy units are given in kcal mol<sup>-1</sup>.

### 10.3 Associative mechanism

In an associative mechanism, a fifth ligand coordinates to Ni-center, giving a 5-coordinate species. This can then undergo a Berry pseudorotation to isomerize the catalyst from one geometric isomer to the other, before finally one ligand leaves to give back to the square planar species (Scheme S10.1c).

We first consider if an external ethylene molecule could serve as the fifth ligand by binding to the Ni-center. The direct optimization using ethylene binding to the Ni-center as an initial guess structure did not yield a stable 5-coordinate species. This species **1-et**, with ethylene unbound (Figure S10.6), is 6.6 kcal mol<sup>-1</sup> uphill with respect to the most stable form of the catalyst **Ni-POP-py 1**. This is due to the unfavorable entropic effect associated with bringing in an additional ethylene molecule to the inner coordination shell of the Ni-metal. The absence of a stable 5-coordinate Ni-species with ethylene bound suggest that the coordination of ethylene to form 5-coordinate species is unlikely.

1-et	1-5coord
$\Delta G = 6.6$	$\Delta G = 1.5$
	
ts-5coord	ts-5coord-c2
$\Delta G^\ddagger = 27.1$	$\Delta G^\ddagger = 28.3$
	

**Figure S10.6.** Optimized structures species involved in isomerization pathway via 5-coordinate Ni-complex. The Gibbs energies are calculated relative to **POP-Ni-py (1)**. Key bond distances are given in Å and angles are given in degrees. Gibbs energy units are given in kcal mol<sup>-1</sup>.

We found that the O-atom of the methoxy group on the ligand can serve as a fifth ligand in coordinating the Ni-center. This species, **1-5coord** (Figure S10.6), is 1.5 kcal mol<sup>-1</sup> higher than catalyst **Ni-POP-py 1** (it is in fact a conformer of catalyst **1**). Two TS conformers for the pseudorotational barriers (**ts-5coord** and **ts-5coord-c2**, Figure S10.6) were found and verified by IRC to be the true TS structures for the isomerization of one catalyst form (catalyst **1**) to its geometric isomer (catalyst **1'**). The lowest energy conformer **ts-5coord** has a barrier of 27.1 kcal mol<sup>-1</sup>, which is lower than the barriers via either 3-coordinate TS (**ts-3coord** at 33.8 kcal mol<sup>-1</sup>, Figure S10.2) or tetrahedral TS (**ts-tet** at 30.8 kcal mol<sup>-1</sup>, Figure S10.5). This is therefore the most likely mechanism: the isomerization of catalyst **Ni-POP-py 1** to its regioisomeric form **Ni-POP-py 1'** occurs via associative mechanism with a proximal OMe group serving as a binding ligand on the fifth coordination site before a pseudoroational TS gives the isomeric catalyst.

#### 10.4 Other possibilities

The loss of P-coordination replaced by methoxy O-coordination was considered. However, the resulting species, **1d** and **1e**, both have very high energy such that their formation is highly endergonic and unfavorable (Figure S10.7). This is perhaps expected as the loss of stronger Ni–P coordination was replaced by weaker Ni–O(methoxy) interaction.

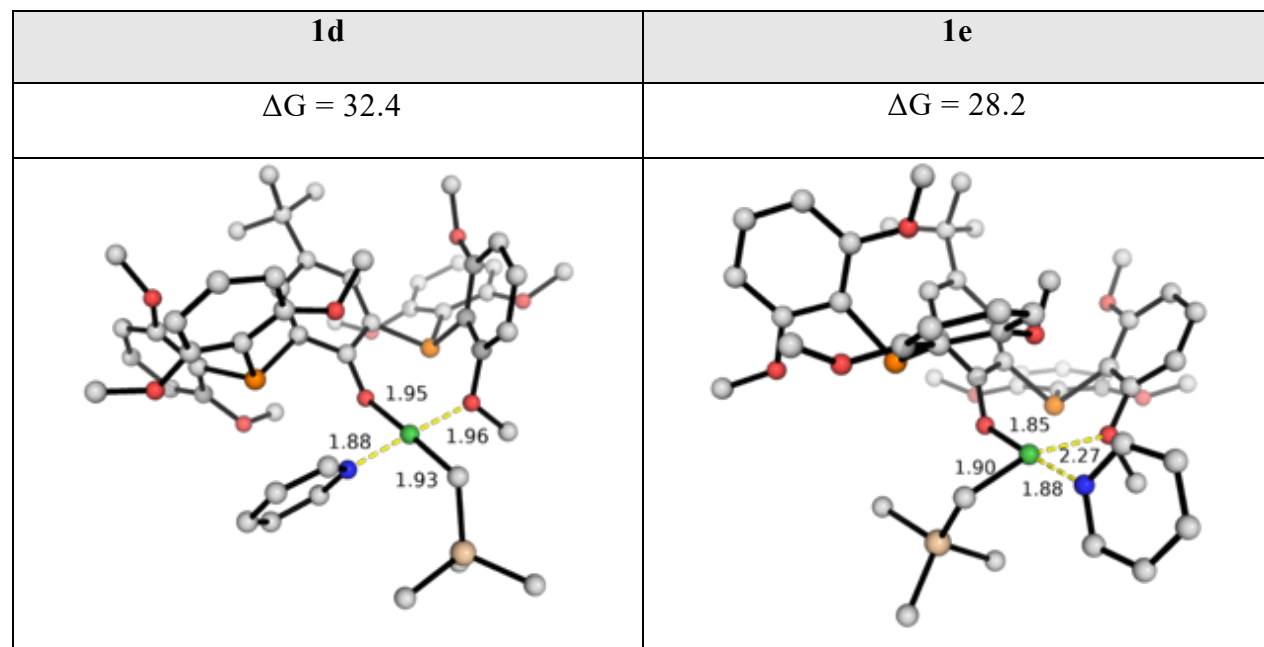
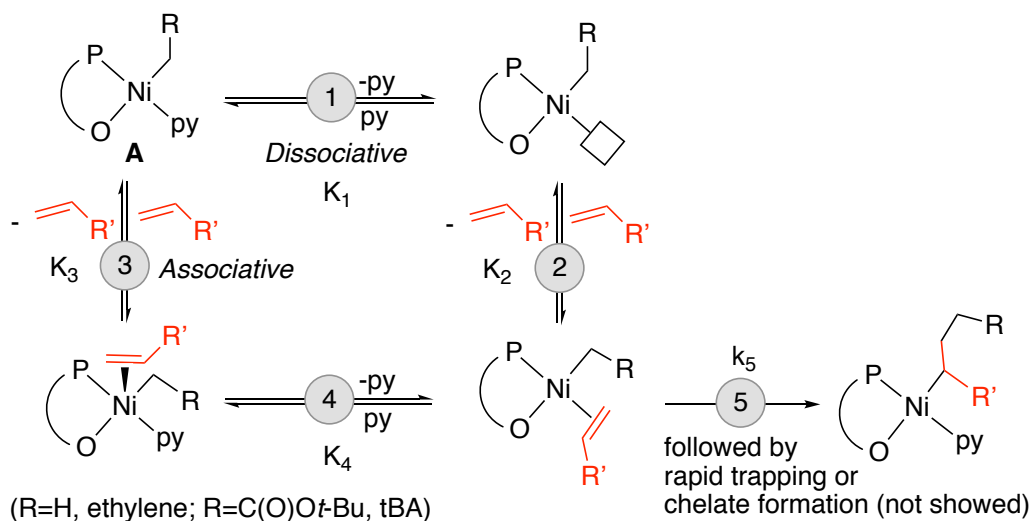


**Figure S10.7.** Optimized structures for the coordination complexes of Ni-catalyst **1** and **1'** where Ni–P interaction is displaced by Ni–O interaction. The Gibbs energies are calculated relative to **POP-Ni-py (1)**. Key bond distances are given in Å. Gibbs energy units are given in kcal mol<sup>-1</sup>.

## 11. Discussion of experimental and computational kinetic studies

### 11.1 Discussion of Enchainment Kinetics (Excluding Potential Isomerization)

The linear dependence indicates that pseudo-1<sup>st</sup> order rate constant ( $k_{obs-1}$ ,  $rate = k_{obs-1}[Ni]$ ) is proportional to the concentration of tBA and inversely proportional to the concentration of pyridine in the range of concentrations studied. To evaluate this behavior, we considered five mechanistic pathways: **A**: Dissociative mechanism and rate determining step pyridine dissociation; **B**: Dissociative mechanism and rate determining step migratory insertion; **C**: Associative mechanism and rate determining step tBA coordination; **D**: Associative mechanism and rate determining step pyridine dissociation; **E**: Associative mechanism and rate determining step migratory insertion. Corresponding rate equation and expressions of rate constants are shown below:



**Path A:** Dissociative mechanism & Rate determining step: pyridine dissociation (Note: tBA is used as the model monomer in this section and following sections. However, the conclusion also works for ethylene or other monomers)

$$\frac{d[A]}{dt} = -k_1 \cdot \frac{k_2[tBA]}{k_{-1}[py] + k_2[tBA]} \cdot [A]$$



$$k_{obs} = k_1 \cdot \frac{k_2[tBA]}{k_{-1}[py] + k_2[tBA]}$$

In this case,

- 1) If  $k_{-1}[py] \gg k_2[tBA]$ ,  $k_{obs} \propto [tBA]/[py]$
- 2) Upper limit of  $k_{obs}$  is  $k_1$
- 3) In the double reciprocal plot (y axis:  $1/k_{obs}$ , x axis:  $[py]/[tBA]$ ), slope =  $1/(k_2K_1)$ , Intercept =  $1/k_1$

**Path B:** Dissociative mechanism & Rate determining step: migratory insertion

$$\frac{d[A]}{dt} = -K_1K_2 \cdot \frac{k_5[tBA]}{[py]} \cdot [A]$$

$$k_{obs} = -K_1K_2 \cdot \frac{k_5[tBA]}{[py]}$$

$$K_{tBA/py} = -K_1K_2$$

In this case,

- 1)  $k_{obs} \propto [tBA]/[py]$
- 2) In the double reciprocal plot (y axis:  $1/k_{obs}$ , x axis:  $[py]/[tBA]$ ), slope =  $1/(K_{tBA/py}k_5)$ , Intercept = 0

**Path C:** Associative mechanism & Rate determining step: tBuAc coordination

$$\frac{d[A]}{dt} = -k_3 \cdot \frac{k_4[tBA]}{k_{-3} + k_4} \cdot [A]$$

$$k_{obs} = k_3 \cdot \frac{k_4[tBA]}{k_{-3} + k_4}$$

In this case,

- 1)  $k_{obs}$  is not related to  $[py]$
- 2)  $k_{obs} \propto [tBA]$
- 3) In the double reciprocal plot (y axis:  $1/k_{obs}$ , x axis:  $[py]/[tBA]$ ), slope =  $1/K_3k_4$ , Intercept = 0 (for different  $[tBA]$ ); or slope = 0, Intercept =  $1/(K_3k_4[tBA]) + 1/(k_3[tBA])$  (for different  $[py]$ )

**Path D:** Associative mechanism & Rate determining step: py dissociation

$$\frac{d[A]}{dt} = -K_3k_4 \cdot \frac{k_5[tBA]}{k_{-4}[py] + k_5} \cdot [A]$$
$$k_{obs} = K_3k_4 \cdot \frac{k_5[tBA]}{k_{-4}[py] + k_5}$$

In this case,

1) If  $k_{-4}[py] \gg k_5[tBA]$ ,  $k_{obs} \propto [tBA]/[py]$

2) If  $k_{-4}[py] \ll k_5[tBA]$ ,  $k_{obs}$  is proportional to  $[tBA]$  but not related to  $[py]$

3) In the double reciprocal plot (y axis:  $1/k_{obs}$ , x axis:  $[py]/[tBA]$ ), slope =  $1/(K_3K_4k_5)$ ,

Intercept =  $1/(K_3k_4)$

**Path E:** Associative mechanism & Rate determining step: migratory insertion

$$\frac{d[A]}{dt} = -K_3K_4 \cdot \frac{k_5[tBA]}{[py]} \cdot [A]$$
$$k_{obs} = -K_3K_4 \cdot \frac{k_5[tBA]}{[py]}$$
$$K_{tBA/py} = -K_3K_4$$

In this case,

1)  $k_{obs} \propto [tBA]/[py]$

2) In the double reciprocal plot (y axis:  $1/k_{obs}$ , x axis:  $[py]/[tBA]$ ), slope =  $1/(K_{tBA/py}k_3)$ ,

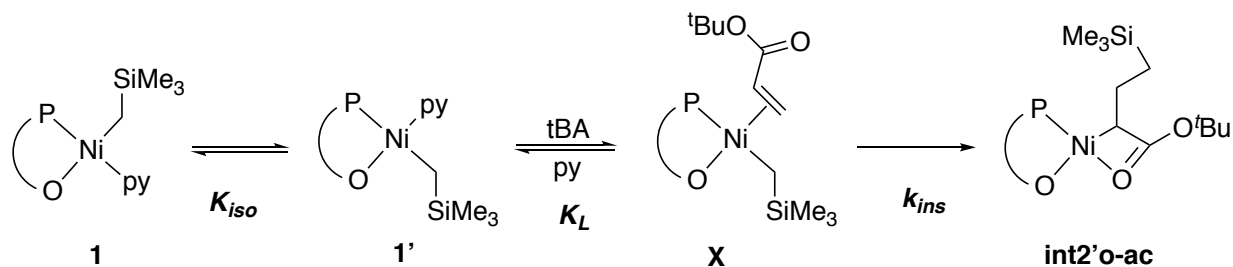
Intercept = 0

Notably, double reciprocal plot is not enough to differentiate path B and path E

Mechanisms A, C, and D are expected to result in non-zero intercepts and therefore are inconsistent with the data. Mechanisms B and E both predict zero intercepts and are consistent with the data. Both of these reaction pathways implicate olefin insertion is slow comparing to ligand exchange (pyridine dissociation + olefin coordination). Note that an isomerization process that moves the alkyl group to the position trans to the phosphine, as previously proposed for asymmetric ligand systems cannot be addressed experimentally as it results in the same dependence on substrate concentration as the above cases (see below).

## 11.2 Discussion of Enchainment Kinetics (Including Isomerization)

Consider the first insertion of either ethylene or tBA. Herein we use tBA as an illustration; note that the case for ethylene will be the same.



The overall rate of the formation of insertion product **int2'o-ac** is given by

$$rate = k_{ins} \cdot [\mathbf{X}] \quad (\text{A})$$

The isomerization step has the highest barrier for this transformation whereas the insertion step is rate-limiting after the isomerization. Applying the steady-state approximation to species **1'**, we have

$$0 = \frac{d[\mathbf{1}']}{dt} = k_{iso} [\mathbf{1}] - k_{-iso} [\mathbf{1}'] + k_{-L} [\mathbf{X}] [\text{py}] - k_L [\mathbf{1}'] [\text{tBA}] \quad (\text{B})$$

Consistent with experimental finding, the insertion step has a slower rate than olefin coordination such that a fast equilibrium exists between species **1'** and **X**. We then have

$$K_L = \frac{[\text{py}][\mathbf{X}]}{[\text{tBA}][\mathbf{1}']} \implies [\mathbf{1}'] = \frac{[\text{py}][\mathbf{X}]}{[\text{tBA}]K_L} \quad (\text{C})$$

where  $K_L$  is the equilibrium constant between species **1'** and **X**.

Substituting Equation (C) into (B), we have

$$\begin{aligned}
0 &= k_{iso} [\mathbf{1}] - k_{-iso} \frac{[\text{py}][\mathbf{X}]}{[\text{tBA}]K_L} + k_{-L} [\mathbf{X}] [\text{py}] - k_L \frac{[\text{py}][\mathbf{X}]}{[\text{tBA}]K_L} [\text{tBA}] \\
\implies [\mathbf{X}] &= \frac{k_{iso}[\mathbf{1}][\text{tBA}]K_L}{k_{-iso}[\text{py}]} = K_{iso}K_L [\mathbf{1}] \frac{[\text{tBA}]}{[\text{py}]}
\end{aligned} \tag{D}$$

Putting Equation (D) in (A), we have the rate of insertion as

$$\begin{aligned}
\text{rate} &= k_{ins} \cdot [\mathbf{X}] = k_{ins}K_{iso}K_L [\mathbf{1}] \frac{[\text{tBA}]}{[\text{py}]} \\
&= k_{ins(\text{tBA})}K_{iso}K_{L(\text{tBA})} [\mathbf{1}] \frac{[\text{tBA}]}{[\text{py}]}
\end{aligned} \tag{E}$$

Similarly, the rate of insertion of ethylene is given by

$$\text{rate} = k_{ins(\text{et})}K_{iso}K_{L(\text{et})} [\mathbf{1}] \frac{[\text{et}]}{[\text{py}]} \tag{F}$$

*Note that equation (E) is consistent with the findings of experiment measurement of tBA enchainment that pseudo-1<sup>st</sup> order rate constant ( $k_{obs-1}$ ,  $\text{rate}=k_{obs-1}[\text{Ni}]$ ) is proportional to the concentration of tBA and inversely proportional to the concentration of pyridine in the range of concentrations studied.*

### 11.3 Comparison of Ethylene and tBA Enchainment

Based on (E) and (F), the relative rate of insertions is then given by

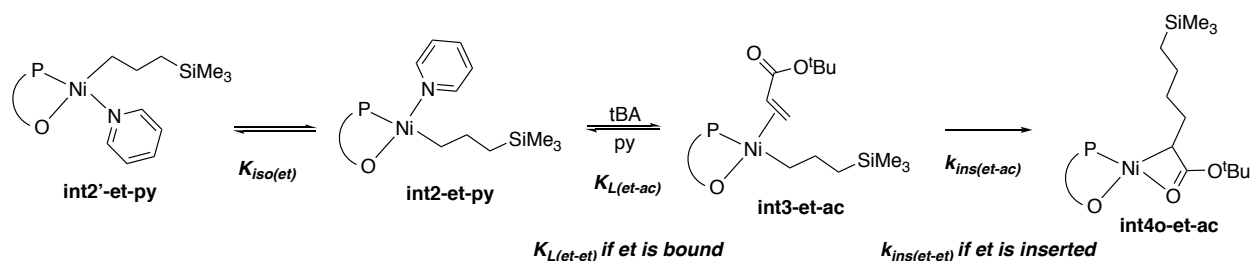
$$\begin{aligned}
\frac{\text{rate}(\text{et})}{\text{rate}(\text{tBA})} &= \frac{k_{ins(\text{et})}K_{iso}K_{L(\text{et})} [\mathbf{1}] [\text{et}]}{k_{ins(\text{tBA})}K_{iso}K_{L(\text{tBA})} [\mathbf{1}] [\text{tBA}]} \\
&= \frac{k_{ins(\text{et})}K_{L(\text{et})} [\text{et}]}{k_{ins(\text{tBA})}K_{L(\text{tBA})} [\text{tBA}]} \\
&= \exp[-\Delta\Delta G^\ddagger/RT] \cdot \exp[-\Delta\Delta G/RT] \frac{[\text{et}]}{[\text{tBA}]}
\end{aligned} \tag{G}$$

where  $\Delta\Delta G^\ddagger = \Delta G_{ins(\text{et})}^\ddagger - \Delta G_{ins(\text{tBA})}^\ddagger$  is the difference between the activation barriers of the insertions and  $\Delta\Delta G = \Delta G_{ins(\text{et})} - \Delta G_{ins(\text{tBA})}$  is the difference between the

complexation/ coordination energies. Note that the barriers are measured for each *elementary step* in this analysis.

For the first insertion of ethylene (Figure S9.9), the barrier of insertion is 5.9 kcal mol<sup>-1</sup> (from **int1'-et-c2** to **ts1'-et**), while the coordination energy is 10.2 kcal mol<sup>-1</sup> (from **1'** to **int1'-et-c2**). For the first insertion of tBA, the barrier of insertion is 3.1 kcal mol<sup>-1</sup> (from **int1'-ac-c4** to **ts1'-ac**), while the coordination energy is 16.2 kcal mol<sup>-1</sup> (from **1'** to **int1'-ac-c4**). Therefore, this gives the difference between the activation barriers of insertion as 2.8 kcal mol<sup>-1</sup> and the difference between the coordination energies as -6.0 kcal mol<sup>-1</sup>. The overall difference in the first insertions of ethylene and tBA is thus (2.8 + (-6.0)) = -3.2 kcal mol<sup>-1</sup>, i.e., the insertion of ethylene has a barrier that is 3.2 kcal mol<sup>-1</sup> lower than the insertion of tBA. This is consistent with the energetic span model<sup>25,26</sup> where the concept of turnover frequency (TOF) determining intermediate (TDI) and TOF-determining transition state (TDTS) is used. For both insertions, the TDI is the catalyst **1'** whereas the insertion step is the TDTS. The barrier differences between the insertion of ethylene (16.1 kcal mol<sup>-1</sup> from **1'** to **ts1'-et**) and the insertion of tBA (19.3 kcal mol<sup>-1</sup> from **1'** to **ts1'-ac**) is 3.2 kcal mol<sup>-1</sup>, consistent with the kinetic analysis above.

Using similar analysis for the second insertion (shown below second insertion of tBA into first ethylene-inserted product as an example), where the key rate-determining steps are the same as for the first insertion,



the relative rates for the second insertion of ethylene (et) vs tBA (ac) into first ethylene-inserted product is given by

$$\begin{aligned}
\frac{\text{rate}(\text{et-et})}{\text{rate}(\text{et-ac})} &= \frac{k_{\text{ins}}(\text{et-et})K_{\text{iso}}(\text{et})K_{\text{L}}(\text{et-et})[\text{int2'-et-py}][\text{et}]}{k_{\text{ins}}(\text{et-ac})K_{\text{iso}}(\text{et})K_{\text{L}}(\text{et-ac})[\text{int2'-et-py}][\text{tBA}]} \\
&= \frac{k_{\text{ins}}(\text{et-et})K_{\text{L}}(\text{et-et})[\text{et}]}{k_{\text{ins}}(\text{et-ac})K_{\text{L}}(\text{et-ac})[\text{tBA}]} \\
&= \exp[-\Delta\Delta G^\ddagger/RT] \cdot \exp[-\Delta\Delta G/RT] \frac{[\text{et}]}{[\text{tBA}]}
\end{aligned} \tag{H}$$

where again the differences between the Gibbs energy of activation  $\Delta\Delta G^\ddagger = \Delta G_{\text{ins}}^\ddagger(\text{et-et}) - \Delta G_{\text{ins}}^\ddagger(\text{et-ac})$  and of complexation/coordination  $\Delta\Delta G = \Delta G_{\text{ins}}(\text{et-et}) - \Delta G_{\text{ins}}(\text{et-ac})$  are similarly defined.

#### 11.4 Comparison of initiation vs propagation of ethylene (or tBA)

The rates of first insertion (initiation) and second insertion (propagation) can be similarly compared. For example, the relative rates of first insertion of ethylene into catalyst **1** and second insertion of ethylene into ethylene-inserted product **int2'-et-py** is given by

$$\begin{aligned}
\frac{\text{rate}(\text{et})}{\text{rate}(\text{et-et})} &= \frac{k_{\text{ins}}(\text{et})K_{\text{iso}}K_{\text{L}}(\text{et})[\mathbf{1}][\text{et}]}{k_{\text{ins}}(\text{et-et})K_{\text{iso}}(\text{et})K_{\text{L}}(\text{et-et})[\text{int2'-et-py}][\text{et}]} \\
&= \frac{k_{\text{ins}}(\text{et})}{k_{\text{ins}}(\text{et-et})} \frac{K_{\text{iso}}}{K_{\text{iso}}(\text{et})} \frac{K_{\text{L}}(\text{et})}{K_{\text{L}}(\text{et-et})} \frac{[\mathbf{1}]}{[\text{int2'-et-py}]} \\
&= \exp\left[-\Delta\Delta G_{\text{ins}}^\ddagger/RT\right] \cdot \exp\left[-\Delta\Delta G_{\text{iso}}/RT\right] \cdot \exp\left[-\Delta\Delta G_{\text{coord}}/RT\right] \cdot \frac{[\mathbf{1}]}{[\text{int2'-et-py}]}
\end{aligned} \tag{I}$$

From the energy profile in Figure S9.9, we see that the barrier for insertion of ethylene into catalyst **1'** (elementary step) is 5.9 kcal mol<sup>-1</sup>; the insertion barrier of ethylene into **int2'-et-py** (Figure S9.11(a)) is 4.6 kcal mol<sup>-1</sup>. This gives a barrier difference in the insertion of 1.3 kcal mol<sup>-1</sup>. Similarly, the barrier difference in isomerization is 22.7 – 18.8 = 3.9 kcal mol<sup>-1</sup>. The difference in the coordination energies is 10.2 – 4.8 = 5.4 kcal mol<sup>-1</sup>. This gives a total barrier difference of 10.6 kcal mol<sup>-1</sup>. Using the energetic span model, the barrier for first insertion is 16.1 kcal mol<sup>-1</sup> from the TDI (**1'**) to TDTS (**ts1'-et**); the barrier for second insertion into first ethylene-inserted product is 9.4 kcal mol<sup>-1</sup> from the TDI (**int2-et-py**) to TDTS (**ts3-et-et**). This gives a barrier difference of 6.7 kcal mol<sup>-1</sup> which is the sum of the

differences in the coordination and insertion energies given by the elementary steps above  $(1.3 + 5.4) = 6.7 \text{ kcal mol}^{-1}$ .

### 11.5 Comparison of propagation of ethylene (or tBA) into ethylene-initiated vs tBA-initiated species

The rates of second insertion (propagation) of each olefin into first ethylene- or tBA-inserted product can be similarly compared. The difference in the rates will arise from the first insertion of ethylene vs tBA, followed by the isomerization in each insertion product, as well as the second insertion into each first insertion product. We consider the insertion of ethylene into ethylene-inserted product vs into tBA-inserted product as an example; the insertion of tBA into ethylene-inserted product vs into tBA-inserted product is similar. The first insertion of ethylene (**ts1'-et**) is more favorable than the insertion of tBA (**ts1'-ac**) by  $3.2 \text{ kcal mol}^{-1}$ . Then, the isomerization of first ethylene-inserted product (**ts-5coord-et**, with a barrier of  $18.8 \text{ kcal mol}^{-1}$ ) is in addition more favorable than the isomerization of first tBA-inserted product (**ts-5coord-ac**, with a barrier of  $22.3 \text{ kcal mol}^{-1}$ ) by  $3.5 \text{ kcal mol}^{-1}$ . The subsequent ethylene insertion into first ethylene-inserted product (**ts3-et-et**, with a barrier of  $9.4 \text{ kcal mol}^{-1}$ ) is in addition more favorable than the tBA insertion into first ethylene-inserted product (**ts3-et-ac**, with a barrier of  $19.3 \text{ kcal mol}^{-1}$ ) by  $9.9 \text{ kcal mol}^{-1}$ . Taken together, this implies that the insertion of ethylene into ethylene-inserted product is *ca.* 10 orders of magnitude faster than into tBA-inserted product.

For the insertion of tBA into first ethylene-inserted vs tBA-inserted product, the insertion of tBA into first ethylene-inserted product (**ts3-et-ac**) has a barrier of  $9.9 \text{ kcal mol}^{-1}$ ; the insertion of tBA into first tBA-inserted product has a barrier of  $20.5 \text{ kcal mol}^{-1}$ . This gives a difference in the insertion step of  $10.6 \text{ kcal mol}^{-1}$ , which is very similar to the difference of insertion of ethylene into first ethylene-inserted and first tBA-inserted product ( $9.9 \text{ kcal mol}^{-1}$  above). The differences in the first insertion of ethylene vs tBA and their subsequent isomerization are the same as above ( $3.2 \text{ kcal mol}^{-1}$  and  $3.5 \text{ kcal mol}^{-1}$  respectively). Thus, we expect the insertion of tBA into tBA-inserted product to be *ca.* 10 orders of magnitude faster than into tBA-inserted product.

## References

- 1) Pangborn, A. B.; Giardello, M. A.; Grubbs, R. H.; Rosen, R. K.; Timmers, F. J. Safe and convenient procedure for solvent purification. *Organometallics* **1996**, *15*, 1518-1520.
- 2) Neuwald, B.; Caporaso, L.; Cavallo, L.; Mecking, S. Concepts for stereoselective acrylate insertion. *J. Am. Chem. Soc.* **2013**, *135*, 1026-1036.
- 3) Low, C. H.; Rosensberg, J. N.; Lopez, M. A.; Agapie, T. Oxidative Coupling with Zr (IV) Supported by a Noninnocent Anthracene-Based Ligand: Application to the Catalytic Cotrimerization of Alkynes and Nitriles to Pyrimidines. *J. Am. Chem. Soc.* **2018**, *140*, 11906-11910.
- 4) Connor, E. F.; Younkin, T. R.; Henderson, J. I.; Waltman, A. W.; Grubbs, R. H. Synthesis of neutral nickel catalysts for ethylene polymerization—the influence of ligand size on catalyst stability. *Chem. Commun.* **2003**, 2272-2273.
- 5) Palmer, W. N.; Zarate, C.; Chirik, P. J. Benzyltriboronates: Building Blocks for Diastereoselective Carbon–Carbon Bond Formation. *J. Am. Chem. Soc.* **2017**, *139*, 2589-2592.
- 6) Bruger, B. J.; Bercaw, J. E. Vacuum line techniques for handling air-sensitive organometallic compounds. *ACS Publications: Experimental Organometallic Chemistry*, Chapter 4, **1987**, pp79-115.
- 7) **Full reference for Gaussian software:**  
Gaussian 16, Revision A.01, Frisch, M. J.; Trucks, G. W.; Schlegel, H. B.; Scuseria, G. E.; Robb, M. A.; Cheeseman, J. R.; Scalmani, G.; Barone, V.; Mennucci, B.; Petersson, G. A.; Nakatsuji, H.; Caricato, M.; Li, X.; Hratchian, H. P.; Izmaylov, A. F.; Bloino, J.; Zheng, G.; Sonnenberg, J. L.; Hada, M.; Ehara, M.; Toyota, K.; Fukuda, R.; Hasegawa, J.; Ishida, M.; Nakajima, T.; Honda, Y.; Kitao, O.; Nakai, H.; Vreven, T.; Montgomery Jr., J. A.; Peralta, J. E.; Ogliaro, F.; Bearpark, M.; Heyd, J. J.; Brothers, E.; Kudin, K. N.; Staroverov, V. N.; Kobayashi, R.; Normand, J.; Raghavachari, K.; Rendell, A.; Burant, J. C.; Iyengar, S. S.; Tomasi, J.; Cossi, M.; Rega, N.; Millam, J. M.; Klene, M.; Knox, J. E.; Cross, J. B.; Bakken, V.; Adamo, C.; Jaramillo, J.; Gomperts, R.; Stratmann, R. E.; Yazyev, O.; Austin, A. J.; Cammi, R.; Pomelli, C.; Ochterski, J. W.; Martin, R. L.; Morokuma, K.; Zakrzewski, V. G.; Voth, G. A.; Salvador, P.; Dannenberg, J. J.; Dapprich, S.; Daniels, A. D.; Farkas, Ö.; Foresman, J. B.; Ortiz, J. V.; Cioslowski, J.; Fox, D. J. Gaussian, Inc., Wallingford CT, 2016.
- 8) Grimme, S.; Bannwarth, C.; Shushkov, P. A Robust and Accurate Tight-Binding Quantum Chemical Method for Structures, Vibrational Frequencies, and Noncovalent Interactions of Large Molecular Systems Parametrized for All Spd-Block Elements (Z = 1-86). *J. Chem. Theory Comput.* **2017**, *13* (5), 1989–2009.
- 9) Manby, F. R.; Miller, T. F.; Bygrave, P. J.; Ding, F.; Dresselhaus, T.; Buccheri, A.; Bungey, C.; Lee, S. J. R.; Meli, R.; Steinmann, C.; et al. Entos : A Quantum Molecular Simulation Package. *ChemRxiv*. **2019**.
- 10) Zhao, Y.; Truhlar, D. G. The M06 Suite of Density Functionals for Main Group Thermochemistry, Thermochemical Kinetics, Noncovalent Interactions, Excited States, and Transition Elements: Two New Functionals and Systematic Testing of Four M06-Class Functionals and 12 Other Function. *Theor. Chem. Acc.* **2008**, *120* (1), 215–241.



- 11) Weigend, F.; Ahlrichs, R. Balanced Basis Sets of Split Valence, Triple Zeta Valence and Quadruple Zeta Valence Quality for H to Rn: Design and Assessment of Accuracy. *Phys. Chem. Chem. Phys.* **2005**, *7* (18), 3297–3305.
- 12) Weigend, F. Accurate Coulomb-Fitting Basis Sets for H to Rn. *Phys. Chem. Chem. Phys.* **2006**, *8* (9), 1057–1065.
- 13) Frisch, M. J.; Trucks, G. W.; Schlegel, H. B.; Scuseria, G. E.; Robb, M. A.; Cheeseman, J. R.; Scalmani, G.; Barone, V.; Mennucci, B.; Petersson, G. A.; et al. Gaussian 16, Revision A.01. 2016.
- 14) Hu, L.; Chen, H. Assessment of DFT Methods for Computing Activation Energies of Mo/W-Mediated Reactions. *J. Chem. Theory Comput.* **2015**, *11* (10), 4601–4614.
- 15) Sun, Y.; Chen, H. Performance of Density Functionals for Activation Energies of Re-Catalyzed Organic Reactions. *J. Chem. Theory Comput.* **2014**, *10* (2), 579–588.
- 16) Sun, Y.; Chen, H. Performance of Density Functionals for Activation Energies of Zr-Mediated Reactions. *J. Chem. Theory Comput.* **2013**, *9* (11), 4735–4743.
- 17) Yu, H. S.; He, X.; Li, S. L.; Truhlar, D. G. MN15: A Kohn–Sham Global-Hybrid Exchange–Correlation Density Functional with Broad Accuracy for Multi-Reference and Single-Reference Systems and Noncovalent Interactions. *Chem. Sci.* **2016**, *7* (8), 5032–5051.
- 18) O’Duill, M. L.; Matsuura, R.; Wang, Y.; Turnbull, J. L.; Gurak, J. A.; Gao, D. W.; Lu, G.; Liu, P.; Engle, K. M. Tridentate Directing Groups Stabilize 6-Membered Palladacycles in Catalytic Alkene Hydrofunctionalization. *J. Am. Chem. Soc.* **2017**, *139* (44), 15576–15579.
- 19) Liu, Z.; Wang, Y.; Wang, Z.; Zeng, T.; Liu, P.; Engle, K. M. Catalytic Intermolecular Carboamination of Unactivated Alkenes via Directed Aminopalladation. *J. Am. Chem. Soc.* **2017**, *139* (32), 11261–11270.
- 20) Fukui, K. Formulation of the Reaction Coordinate. *J. Phys. Chem.* **2005**, *74* (23), 4161–4163.
- 21) Fukui, K. The Path of Chemical Reactions - The IRC Approach. *Acc. Chem. Res.* **1981**, *14* (12), 363–368.
- 22) Marenich, A. V.; Cramer, C. J.; Truhlar, D. G. Universal Solvation Model Based on Solute Electron Density and on a Continuum Model of the Solvent Defined by the Bulk Dielectric Constant and Atomic Surface Tensions. *J. Phys. Chem. B* **2009**, *113* (18), 6378–6396.
- 23) Grimme, S. Supramolecular Binding Thermodynamics by Dispersion-Corrected Density Functional Theory. *Chem.: Eur. J.* **2012**, *18* (32), 9955–9964.
- 24) Funes-Ardoiz, I.; Paton, R. S. GoodVibes v1.0.1 <http://doi.org/10.5281/zenodo.56091>.
- 25) Contreras-García, J.; Johnson, E. R.; Keinan, S.; Chaudret, R.; Piquemal, J. P.; Beratan, D. N.; Yang, W. NCIPLOT: A Program for Plotting Noncovalent Interaction Regions. *J. Chem. Theory Comput.* **2011**, *7* (3), 625–632.
- 26) Sosa, C.; Andzelm, J.; Elkin, B. C.; Wimmer, E.; Dobbs, K. D.; Dixon, D. A. A Local Density Functional Study of the Structure and Vibrational Frequencies of Molecular Transition-Metal Compounds. *J. Phys. Chem.* **1992**, *96* (16), 6630–6636.

- 27) Godbout, N.; Salahub, D. R.; Andzelm, J.; Wimmer, E. Optimization of Gaussian-Type Basis Sets for Local Spin Density Functional Calculations. Part I. Boron through Neon, Optimization Technique and Validation. *Can. J. Chem.* **1992**, *70* (2), 560–571.
- 28) Schrödinger, L. *The PyMOL Molecular Graphics Development Component, Version 1.8*; 2015.
- 29) Guironnet, D.; Roesle, P.; Rünzi, T.; Göttker-Schnetmann, I.; Mecking, S. Insertion Polymerization of Acrylate. *J. Am. Chem. Soc.* **2009**, *131* (2), 422–423.
- 30) Ito, S.; Munakata, K.; Nakamura, A.; Nozaki, K. Copolymerization of Vinyl Acetate with Ethylene by Palladium/ Alkylphosphine-Sulfonate Catalysts. *J. Am. Chem. Soc.* **2009**, *131* (41), 14606–14607.
- 31) Noda, S.; Nakamura, A.; Kochi, T.; Lung, W. C.; Morokuma, K.; Nozaki, K. Mechanistic Studies on the Formation of Linear Polyethylene Chain Catalyzed by Palladium Phosphine-Sulfonate Complexes: Experiment and Theoretical Studies. *J. Am. Chem. Soc.* **2009**, *131* (39), 14088–14100.
- 32) Amatore, C.; Jutand, A. Mechanistic and Kinetic Studies of Palladium Catalytic Systems. *Journal of Organometallic Chemistry*. Elsevier March 15, 1999, pp 254–278.
- 33) Kozuch, S.; Shaik, S. How to Conceptualize Catalytic Cycles? The Energetic Span Model. *Acc. Chem. Res.* **2011**, *44* (2), 101–110.